City Research Online

City, University of London Institutional Repository

City Research Online: http://openaccess.city.ac.uk/   publications@city.ac.uk

Coupling a local adaptive grid refinement technique with an interface sharpening scheme for the simulation of two-phase flow and free-surface flows using VOF methodology.

Ilias Malgarinos[1*], Nikolaos Nikolopoulos[1,2] and Manolis Gavaises[1]

1: School of Engineering and Mathematical Sciences, City University London, Northampton Square, EC1V 0HB London, UK, *Corresp. Author – e-mail: Ilias.Malgarinos.1@city.ac.uk

2: Centre for Research and Technology Hellas, Chemical Process and Energy Resources Institute, Egialeias 52, Marousi, Athens, Gr-15125, Greece

1: School of Engineering and Mathematical Sciences, City University London, Northampton Square, EC1V 0HB London, UK

Abstract

This study presents the implementation of an interface sharpening scheme on the basis of the Volume of Fluid (VOF) method, as well as its application in a number of theoretical and real cases usually modelled in literature. More specifically, the solution of an additional sharpening equation along with the standard VOF model equations is proposed, offering the advantage of "restraining" interface numerical diffusion, while also keeping a quite smooth induced velocity field around the interface. This sharpening equation is solved right after volume fraction advection; however a novel method for its coupling with the momentum equation has been applied in order to save computational time. The advantages of the proposed sharpening scheme lie on the facts that a) it is mass conservative thus its application does not have a negative impact on one of the most important benefits of VOF method and b) it can be used in coarser grids as now the suppression of the numerical diffusion is grid independent. The coupling of the solved equation with an adaptive local grid refinement technique is used for further decrease of computational time, while keeping high levels of accuracy at the area of maximum interest (interface). The numerical algorithm is initially tested against two theoretical benchmark cases for interface tracking methodologies followed by its validation for the case of a free-falling water droplet accelerated by gravity, as well as the normal liquid droplet impingement onto a flat substrate. Results indicate that the coupling of the interface sharpening equation with the HRIC discretization scheme used for volume fraction flux term, not only decreases the interface numerical diffusion, but also allows the induced velocity field to be less perturbed owed to spurious velocities across the liquid-gas interface. With the use of the proposed algorithmic flow path, coarser grids can replace finer ones at the slight expense of accuracy.

Keywords: CFD; VOF; interface sharpening; adaptive grid; droplet acceleration

Nomenclature

Symbol	Quantity	units	Greek letters		
$\vec{\alpha}$	acceleration	m/s^2	α	Liquid volume fraction	
A	surface	m^2	B	Sharpening intension constant	(-)
C$_d$	Drag Coefficient	(-)	Δρ	ρ_{liq}-ρ_{gas}	Kg/m^3
C$_p$	Pressure Coeff.	(-)	Δx	cell width	m
cpR	Equiv. cells where R is resolved		Δt	Time-step	(s)
D	Droplet Diameter	m	E	Interface thickness constant	(-)
Eo	Eotvos number	(-)(=g$\Delta\rho d_{liq}^2/\sigma$)	K	curvature	1/m
$\vec{f}_\sigma$	Surface Tension	N/m^3	M	dynamic viscosity	kg/ms
F	force	Nt	ρ	density	kg/m^3
$\vec{g}$	Gravitational acceleration	m/s^2	σ	surface tension coefficient	N/m
M	mass	kg	Tα	Pseudo-time	
Mo	Morton number	(-) (=g$\mu_{air}^4\Delta\rho/\rho_{air}\sigma^3$)	Φ	Phi variable	
$\hat{n}$	Free-surface normal	(-)	Ψ	Stream Function	(1/s)
$\vec{n}$	Face normal vector	(-)	Ω	Rotational Velocity	(1/s)
P	Pressure	Pa	**Subscripts**		

Re	Reynolds number	$(-)(=\rho u D/\mu)$	D	Drag	
T	time	s	Gas	gas	
$\vec{\vec{T}}$	Stress tensor		Liq	liquid	
$\vec{u}$ (u,v,w)	Velocity (its components)	m/s	O	initial condition	
V	volume	m^3	Term	terminal	
We	Weber number	$(-)(=\rho_{liq} u D/\sigma)$	**Superscripts**		
X	x-axis distance	m	N	Random time instant	
Y	x-axis distance	m	**Abbreviations**		
			TVD	Total Variation Diminishing	

1. Introduction

The interaction between liquid and gaseous phases appears in many technological applications. Complex phenomena such as droplet motion, collision, wall impingement, coupled with phase change (condensation or evaporation) are apparent in a vast number of industrial areas ranging from power plant steam condensation units [1, 2] and internal combustion engines [3] to spray cooling [4] and anti-icing of airfoils [5].

CFD simulations have been used for investigating such phenomena for the past five decades, since Francis Harlow and Eddie Welch in 1965 first published a CFD algorithm for solving the Navier-Stokes equations governing the motion of free-surfaces [6]. Since then, a vast number of studies dealing with such phenomena, i.e. the simulation of liquid-gas interfaces, have been published while numerous and of different background approaches have been setup and tried up to day showing respective advantages and disadvantages. The most representative such approaches concern a) the *Lagrangian* algorithm (selectively one can refer to the marker cell [7], deforming grid [8, 9], front tracking [10, 11], LCRM [12]), the *Eulerian* algorithm (SOLA-VOF [13-15], Volume of Fluid Method (VOF) [16-19], CLSVOF [20], Level Set [21, 22], VOF+PLIC [23], PLIC, VOF with Youngs reconstruction [24, 25]) and the *Eulerian-Lagrangian* coupled approaches [26, 27].

In the framework of this study, among the aforementioned interface tracking schemes, the Volume of Fluid Method (VOF) is used, since this is known to exhibit good mass conservation, and to have the ability to handle significant topology changes as in the case of liquid mass elongations. The latter feature is considered to be of high value requirement for any droplet dynamics prediction tool. However, a typical VOF scheme has deficiencies in calculating a smooth surface tension force along the liquid-gas interface

and under several conditions induces high numerical diffusion [28]. The aim of this study is to implement a robust numerical algorithm that deals with the latter problem.

Up to now, in recent literature, two basic paths are usually followed, in order to remedy the problem of artificial diffusion imposed by the standard VOF method. The first is to implement very accurate advection algorithms and the second to utilize algorithms that explicitly suppress any numerical diffusion and restrict the interface region to the minimum possible number of numerical cells. Referring to the first approach, because in Eulerian approaches the exact location of the interface is not known, a reconstruction procedure is absolutely required in order to advect the liquid phase from one cell to its neighbor during one time-step. For that reason, special discretization schemes for the volume fraction equation flux term are used in order to make that reconstruction more accurate. Such schemes include, for example the CICSAM [29], the HRIC [30], the PLIC [24] and/or THINC [20]. Nevertheless, again problems usually arise in under-resolved regions of the computational grid, especially at regions where the liquid phase changes direction in an abruptly way. Moreover, the application of different discretization schemes for the same conditions (similarly setup cases) most of the times can reveal significant differences, thus proving that the choice of any discretization scheme for the liquid phase advection is very important in terms of accurate representation of physical phenomena by mathematical models. For example, in Figure 1, the basic differences of two discretization schemes, namely CICSAM and HRIC are presented for the real case of a water droplet acceleration under the influence of gravity. In this Figure, the characteristics of the induced velocity field along the interface spatial distribution are presented.

The CICSAM [29] discretization scheme, which is highly non-diffusive, predicts unrealistic velocity values at the interface (Figure 1a-red spots on the interface), which in turn gives rise to non-physical velocity magnitude and pressure predictions inside the liquid phase. On the other hand, the HRIC discretization scheme [30], which is a TVD (Total Variation Diminishing) high resolution scheme of a nonlinear blending of upwind and downwind differencing schemes, produces more smooth velocity field components and perhaps more reasonable (perhaps stand for the reason there are not any real measurements to compare with). However, HRIC highly diffuses the interface as it can be seen in Figure 1b. A comparison of the behavior between these two discretization schemes in a number of benchmark cases is also presented by Waclawczyk and Koronowicz [31], who reached to similar conclusions. It is thus understood that the application of a method capable of combining the advantages of each of these two aforementioned discretization schemes, would be a real benefit for any type of VOF simulation.
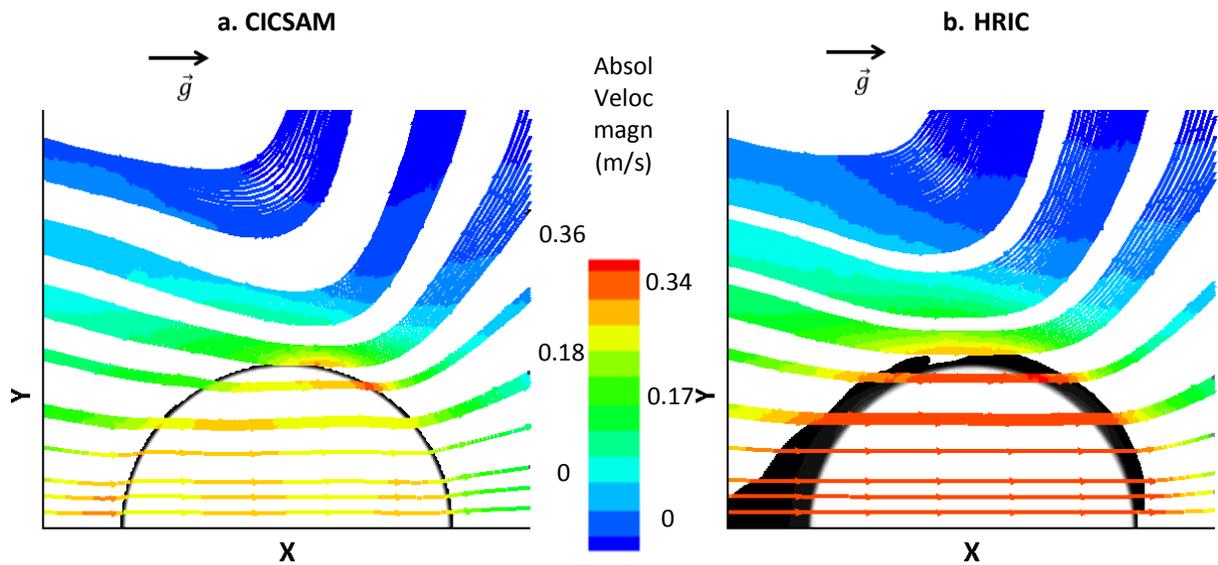
Figure 1. Comparison between a) CICSAM and b) HRIC discretization schemes for predicting the absolute velocity of a free-falling droplet after 30ms of simulation time (initial zero velocity). The volume fraction field is also plotted (gray-scale). Volume fraction values between 0.001 and 0.999 are shown.

On the other hand, the alternative way to suppress the numerical diffusion is to apply a sharpening algorithm, meaning an algorithm which explicitly minimizes the interface region. The last decade, special attention has been paid to such algorithms, which are explicitly used, in order to keep the diffusion of volume fraction field at low levels, while liquid advection is discretized by discretization schemes of lower order of accuracy. Olsson and Kreiss in 2005 [32, 33] proposed a sharpening equation, which is solved right after the advection of the liquid phase (they refer to it as the re-initialization step) in order to avoid diffusion and achieve mass conservation in Level Set simulations. They validated their algorithm in the case of an oscillating droplet both in two and three dimensions. Sato and Niceno [34] used the same equation, however enhanced it with a parameter that controls deformation according to the direction of interface velocity. So, based on their model, the sharpening equation does not have the same intensity across the interface. The authors validated their algorithm in a wide range of cases including those of the dam breaking problem and the rising bubble in a viscous liquid. Most recently, Shukla et al. [35] using a modification of the Olsson's equation, applied the sharpening algorithm in very interesting compressible shock-capturing cases. Similar numerical schemes are also used by other groups in order to simulate two-phase flow phenomena. Weller, in 2008 [36], introduced an additional convective term (he refers to it as the 'compression term') in volume fraction equation, which is similar to one term of Olsson's equation, and coupled it with a 'compression velocity' that accounts for the direction of possible diffusion. Berberovic [37] used the same scheme in order to simulate droplet impingement on a heated wall. So et al. [38] solved an anti-diffusion equation after liquid phase advection, which contains a similar term to Olsson's equation, however they discretized this term using the minmod limiter in order to achieve both mass conservation of the liquid phase and boundedness of the volume fraction values. They also applied their methodology to compressible two-phase flows afterwards [39]. Finally, in a very interesting work, Lentine et al. [40] used a numerical sharpening procedure right after a semi-Lagrangian advection using very large time-step in order to correct the smeared out color function field. Therefore, it seems that the implementation of a sharpening algorithm is promising since on one hand is solved explicitly after liquid phase advection, and on a second hand can be coupled with all possible liquid advection algorithms used.

Furthermore, such types of techniques seem to be straightforwardly applied to unstructured grids and not affected by on grid orientation and grid size.

Therefore, the main motivation of the current study is to implement such a sharpening scheme in the standard VOF model, and couple it with the HRIC discretization scheme for the volume fraction advection. In this way, the smooth velocity field achieved by the HRIC discretization scheme (Figure 1) can be paired with a sharp interface.

2. Methodology

2.1 Volume of Fluid Method

For interface-tracking, the Volume of Fluid method (VOF) is used, which is appropriate for the simulation of flow between two immiscible fluids. In the VOF model, which was first proposed by Hirt and Nichols [41], the full Navier-Stokes equations for mass and momentum conservation are solved, together with the advection of a scalar quantity, named as color function or volume fraction (α) which is used in order to follow the motion of the one phase. These equations are presented below:

$$\frac{\partial \rho \vec{u}}{\partial t} + \nabla \cdot (\rho \vec{u} \otimes \vec{u} - \vec{T}) = \rho \vec{g} + \vec{f}_\sigma \tag{1}$$

$$\frac{\partial \alpha}{\partial t} + \nabla \cdot (\vec{u}\alpha) = 0 \tag{2}$$

These equations, namely momentum conservation equation (eq. 1) and volume fraction advection (eq. 2), are the standard ones for VOF simulations can be as well found in [42, 43]. Regarding liquid-gas simulations, which will be used in the present study, the volume fraction α, takes the value of zero (0) if the computational cell is covered only by gas phase, and the value of one (1) if the cell is completely covered by liquid. For in-between values, the cell lies in a region called the "interface" between the two fluids.

The fluid properties in momentum equation (eq. 1) are updated according to the volume fraction value of the cell, namely as:

$$\mu = \alpha \mu_{liq} + (1-\alpha)\mu_{gas} \; , \; \rho = \alpha \rho_{liq} + (1-\alpha)\rho_{gas} \tag{3}$$

Surface tension term $\vec{f}_\sigma$ is approximated as a volumetric force, taken from the work of Brackbill et al. [44], as

$$\vec{f}_\sigma = \sigma \frac{\rho \kappa \nabla \alpha}{\frac{1}{2}(\rho_{liq} + \rho_{gas})} \tag{4}$$

, where "κ" is the curvature of the free surface and is approximated as the divergence of unit surface normal "n", i.e.

$$\kappa = \nabla \cdot \hat{n} \; , \; \hat{n} = \left(\frac{\nabla \alpha}{|\nabla \alpha|}\right) \tag{5}$$

For a more accurate calculation of curvature, the unit surface normal vectors at the computational nodes are used. Pressure–velocity coupling is achieved by the PISO algorithm. Discretization of the momentum flux term is achieved by a second-order upwind scheme, while for the time discretization a first-order implicit approach is followed for the momentum equation. The volume fraction equation is solved in an explicit manner at the beginning of each time-step using as an input the velocity values derived during the previous time step.

In the case of the droplet impingement on a solid surface, where the wettability of the wall needs to be accounted for, a similar approach to the one presented in Brackbill et al. (eq. 53) [44] and Ubbink (eq. 2.22) [29] is followed. The normal to the interface unit vector at the wall boundary cells $\hat{n}$ is rotated, according to the prescribed value of the contact angle θ, and the following equation:

$$\hat{n} = \hat{n}_w \cos\theta + \hat{n}_t \sin\theta$$

(6)

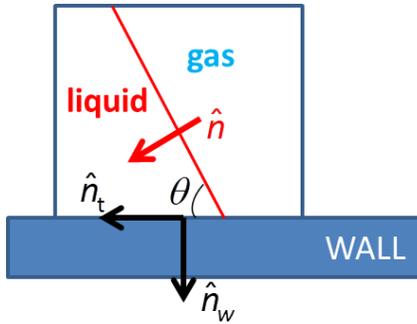Figure 2 is presented for better understanding of eq.6 concept and notation.

Figure 2. Unit vectors on the wall face, as well as unit free surface normal vector.

For the volume fraction flux term, in this study, the CICSAM [29] and the HRIC [30] discretization schemes are used. CICSAM has been proved to be a reliable tool for the prediction of various two-fluid phenomena concerning a) droplet impingement onto a wall film, b) binary droplet collisions and c) droplet impingement onto heated surfaces, as presented in previous works [42, 45, 46] [18, 19, 43, 47, 48] published by authors who belong to the same research group as the authors of this study. On the other hand HRIC scheme achieves to have a smoother velocity field and avoids the induction of excessive spurious velocities at the interface. The commercial package of ANSYS FLUENT is chosen for the solution of these equations.

2.2   Interface Sharpening Algorithm

The solution of an additional, sharpening equation, which was first proposed by Olsson et al. [32], adopted by Sato and Niceno [34] and Shukla et al. [35] and mostly used in Level-Set simulations is proposed in this study in order to keep a sharp interface. The applied pseudo-equation is:

$$\frac{\partial \varphi}{\partial \tau} + \beta \nabla \cdot \varphi((1-\varphi)\hat{n}) = \beta \varepsilon \nabla \cdot (\nabla \varphi)$$

(7)

, where φ is the volume fraction field taken right after VOF advection, ε is a sharpening constant which controls the thickness of the interface, τ is pseudo-time and β is a constant proposed by Sato and Niceno [34] in order to avoid free-surface shape deformation. In their work, this constant is reported to take values in the range from 0.01 to 1. On the contrary, in this study, β is set equal to 1 throughout the domain,

which by a number of numerical tests undertaken, under the specific setup, is proven to aid both in preserving a sharp interface, as well as a mass conservative volume fraction field.

This equation has three terms, namely a) the temporal, b) the flux ('compression term') and c) the diffusion ('artificial diffusion term') terms. However, it is neither written in conservative form nor has any physical meaning. It is used as a 'correction' of the volume fraction field. As Shukla et al. [35] state, this equation "restores, or regularizes, the missing immiscibility condition of the two fluids". If one takes a closer look at the flux and diffusion terms, it is easily deduced that these terms change sign across the interface. In this way, the flux term 'compresses' the interface (values below 0.5 will get smaller, while values above 0.5 will tend to get higher), while the diffusion term has the opposite behavior.

By the use of this equation, the updated values of the 'corrected' volume fraction field are controlled by the value of ε, which in mathematical terms reflects the amount of diffusion added to the initial volume fraction field (after the solution of the standard volume fraction equation). Numerically, equation 7 can be solved after volume fraction advection, and right before the solution of the momentum and pressure correction equations, as stated in previous works [32-35]. In this way, the momentum equation solved contains the 'corrected' values of the volume fraction field. Based on our numerical tests, it is derived that if this equation is solved at the end of the time-step, meaning in other words that the momentum equation is solved with the properties weighted over the 'diffused' volume fraction field (before the sharpening procedure), no significant impact on the numerical results is identified. In other words, this approach reveals that the effect of the sharpening equation on the induced flow field is not considerable, minding that the correction is still conducted, but with a time lag. So, in order to be more efficient, and since for the simulations presented in this paper, the volume fraction field is updated at the beginning of the time-step (explicit calculation), the sharpening equation is solved coupled with the momentum equation and the resulting 'corrected' volume fraction values are patched to the volume fraction field at the end of the time-step. By that measn, the advection in the next time-step will commence on a diffusion-free basis. This equation is solved in pseudo-time (First-Order Implicit discretization in time), while the time-step is selected to be equal to the advection time-step.

Variable ε, in eq. 7, takes the value of $\Delta x/2$ (where Δx is the grid cell edge, as proposed by Sato and Niceno [34]) and moderate sharpening is achieved. This choice will be hereinafter referenced as SHARP (Sharpening). In order to achieve an even sharper interface; a value equal to $\Delta x/3$ is as well examined, hereinafter referred as High Sharpening-HSHARP. Though HSHARP achieves intense interface sharpening, this choice is proven to lack in terms of mass conservation, and in order to restore mass balance of the liquid phase, a simple mass conservation algorithm is proposed and applied. This mass conservation algorithm is presented in a following section (2.4).

The term $(1-\phi)\cdot\hat{n}$ is approximated using central differences as proposed by Olsson et al. [33], while the ϕ equation is solved using the QUICK discretization scheme, a choice which is proven to be beneficial for the mass conservation of the method. At boundary faces, the flux term of this equation is set to zero, in order to "avoid any flow through the boundaries" as Olsson and Kreiss state in their work [33]. In the case of liquid spreading on a solid surface, the wettability of the surface needs to be accounted for. Therefore, it is of high importance in a numerical algorithm that a) the sharpening procedure is executed along the direction of the prescribed contact angle and b) the application of the sharpening scheme does not affect the solution near the wall boundary. Zahedi et al. [49] have dealt with this problem with introducing a regularized normal vector $\tilde{n}$, which is derived from the solution of an equation containing the actual $\hat{n}$. This equation is solved using Dirichlet boundary condition that accounts for the contact angle. Moreover, they introduce another term in eq. 7 that accounts for the tangential diffusion of the interface. In a recent work, Sato and Niceno [50] set the normal to the wall component of vector $\hat{n}$ equal to zero in "wall layer

cells", so that the sharpening procedure will act only towards the tangential to the wall direction. Moreover, they enforce the second and third terms in eq. 7 to be zero for the faces that are parallel to the wall boundary on "wall layer cells", minding a Cartesian grid. A major drawback of this method is that it is not easily and straightforward applicable in an unstructured grid, especially in the case of triangular elements.

On the other hand, study proposes a simpler approximation which is easily applicable on unstructured grids, while the conservation of the volume fraction field is preserved based on numerous simple test cases we performed. More specifically, the unit normal vector $\hat{n}$ which is used in eq. 7 and gives the sharpening direction, for the cells neighboring to wall boundary is altered based on eq. 6, following a similar procedure as for the curvature calculation afore-presented. However, this was not enough to enforce the contact angle boundary condition. Therefore, in addition to that, β takes the value of 0.25 throughout the domain. In this way, the effect of the sharpening procedure to the volume fraction field (which is defined by contact angle boundary condition, eq. 6) is lower and the droplet rim is enforced to adjust to the prescribed contact angle value, which for β > 0.25could not happen. In future works, a local value of 0.25 can be applied near the three-phase contact line, while β=1 throughout the remaining domain.

The implementation of this equation in the commercial code ANSYS FLUENT is achieved using a User Defined Scalar, for which flux and temporal terms are calculated by User Defined Functions (UDFs). An outline of this equation insertion under the platform of ANSYS FLUENT solver is presented in Figure 3.
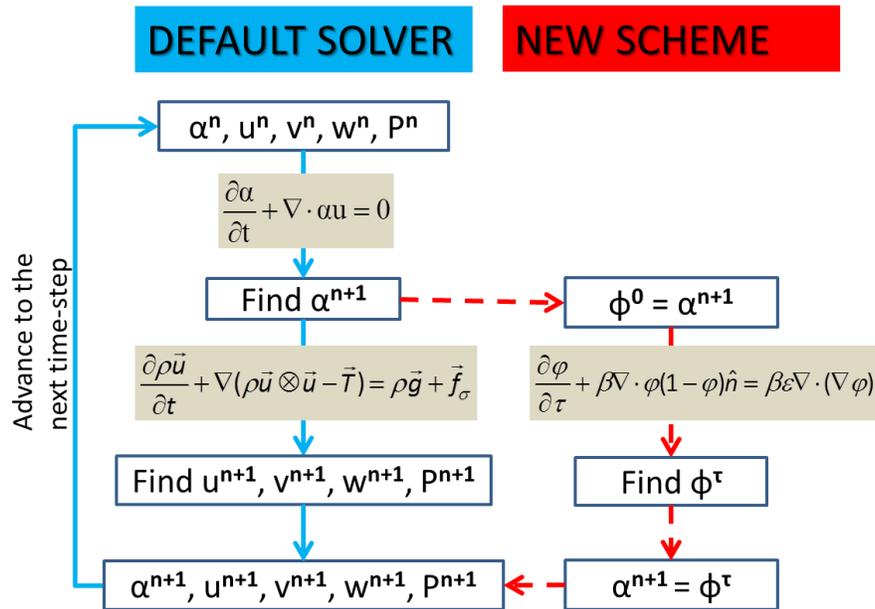

Figure 3. Outline of the Sharpening scheme used.

It is noticeable that such an algorithmic route decreases the required actual computational time, as this equation is neither solved before the momentum solution as in previous works [32-35], nor at the end of each time-step.

2.3   Local Refinement Technique

In order to save further computational time, a local refinement technique is as well proposed based on the work of Theodorakakos and Bergeles [51]. According to this, which has been validated for a wide range

of different cases [18, 42, 48], the mesh is dynamically refined at a prescribed distance from the interface, so that the numerical accuracy of the results can be as high as possible with the minimum computational cost. Numerically, the implementation of this technique is achieved by a) looping over all cells of the domain once, b) finding the isoline of α=0.5 and then c) looping over the cells as many times as the isoline cells in order to find their distance from the interface. As a last step, the cells that lie within the user-specified distance from the interface are marked for refinement. In this work, this distance is selected to be $D_0/6$, which is found to be far enough from the interface, so that the VOF gradients and curvature always lie in the region with the smallest cells. The local refinement technique is applied every 20 time-steps, so that the interface never exits the finest level of refinement cells.

Since such grid treatment is not given as a standard user option in ANSYS/FLUENT software, the implementation of this technique is achieved through numerous User Defined Functions (UDFs), which run at the end of each time-step. The method of grid refinement is based on the hanging node adaption, available in ANSYS FLUENT.

At this point, it is very important to notice that there is basic difference between the dynamic local grid refinement technique which is presented in this study and the work of Theodorakakos and Bergeles [51]. That is linked with the coarsening step applied at the local refined grid. In their work, when the refinement technique is applied, the computational grid is decomposed until the initial grid level is reached and then it is refined again at the region where it is appropriate. During every coarsening and refinement procedure, smoothing of all flow field values is executed. On the other hand in this work, only the cells which should be refined, and the ones that should be coarsened according to the mark for refinement variable change. All other cells remain the same. Therefore, smoothing is executed only at the limits of the refined region, far enough to retain accuracy levels high, thus achieving as well a significant decrease of the actual time of computations.

2.4   Mass Conservation Algorithm

For the case of the High Sharpening (HSHARP) scheme (ε=Δx/3), the total mass of volume fraction is not conserved, and for that reason a simple mass conservation algorithm is used at the end of time-step in order to keep the total liquid mass constant. According to this algorithm, based on two values that define the interface, the upper limit and lower limit (in this study the values of 0.1 and 0.9 respectively are used), if the total mass is lower than the initial one (for cases without mass source/sink) then the following steps are followed; i.e. i) liquid mass is added to all droplet interior cells, which are defined those cells where all of their neighboring cells have values larger than the upper limit and ii) the rest of the mass (if any) is added to the interface cells. The amount of mass which is added in every cell is always based on a) the amount of mass which is missing (mass missing = correct mass − current mass), and b) the maximum allowable liquid mass which can be added (an amount of $(1-\alpha_{cell})\rho V_{cell}$) for each cell. The total mass added in each cell therefore equals to:

$$\alpha_{cell\,NEW} = \alpha_{cell} + (1\text{-}\alpha_{cell})[\sum_{cells}(1-\alpha_{cell})\rho V_{cell}\,/\,mass\text{ missing}] \qquad (8)$$

The necessity for this algorithm is important, given the fact that if one omits that mass correction step, 0.04% of initial liquid mass is lost at each time step, at least for the cases examined in this paper. In other words for every ms of real calculation the liquid mass decreases by around to 3.7%.

3. Results and Discussion

The main motivation of the current study, is to couple a sharpening algorithm with the standard HRIC discretization scheme, used in volume fraction advection term, in order to achieve a smooth velocity field along with a sharp interface. In order to evaluate the performance of this algorithmic path, firstly its direct comparison against the standalone HRIC discretization scheme is needed, so that the effect of the sharpening procedure can become obvious. Secondly, its comparison against a "highly non-diffusive" standalone discretization scheme should be evaluated, in terms of the induced velocity field characteristics (degree of uniformity) and color function diffusion, such as the one depicted in Figure 1. For the choice of "non-diffusive" scheme, CICSAM was selected. Such a choice does not imply that CICSAM behaves better than other open literature discretization schemes, or the ones available in ANSYS FLUENT commercial software, as for example Geo-Reconstruct. Geo-Reconstruct is a discretization scheme which is based on a piece-wise linear interpolation used for the calculation of volume fraction gradient needed for the flux term of the volume fraction equation. Nevertheless, the performance of Geo-Reconstruct for the cases examined in this work and the reasons why it was not further used in the current framework are presented in Appendix A. In the cases which are accompanied by the sharpening step, either default sharpening-SHARP or high sharpening-HSHARP is used. For the easiness of the reader, the abbreviations which are used in the rest of the study and summarize the different methods tested are CICSAM, HRIC, HRIC+SHARP, HRIC+HSHARP.

At first two basic theoretical numerical benchmark cases, i.e. a) the Zalesak's Disk and b) the Single Vortex in a deformation field are examined as a reference, and subsequently two actual cases of interacting droplets with gas environments are examined. The first is the droplet free falling under the influence of gravity, whilst the second is the droplet impingement onto a solid substrate. Especially, the real case of the free falling droplet is considered to be a difficult one from a numerical point of view, since its main difficulty lies on the exact prediction of the induced velocity and pressure profiles exerted on the continuously accelerating droplet interface and to the best of authors knowledge not much information in the literature on such type of simulations exist. In such a case the prediction of any non-smoothed and diffused unrealistic interface accompanied by highly spurious velocity/pressure profiles around it, results in an under/over prediction of drag and lift coefficients of any deformable liquid mass within a continuous gas flow stream, which in turn leads to the failure of the method to correctly represent the physically evolving phenomenon.

Finally, the benchmark cases are tested both on a standard uniform grid and a dynamic one, where grid density topology varies according to the afore-described use of the dynamic local grid refinement technique, in order to validate that use of the local grid refinement technique does not affect the results. The real cases were all run using this dynamic local grid refinement technique.

3.1   Benchmark Cases

3.1.1   Zalesak's Disk

At first, the new algorithm is tested for the conditions of Zalesak's disk [52]. In this Case a slotted disk, centered at (0.5,0.75) in a unit square domain is subjected to rotation under the influence of a stationary vortex field. Initial disk dimensions and domain which are used for the simulation are presented in Figure 4, while the stationary velocity components for the two dimensions are given by:

$$u(x) = -\Omega \cdot (y - 0.5)$$

(9)

$$v(y) = \Omega \cdot (x - 0.5)$$

(10)

, where Ω is the rotation velocity, taken equal to $\pi/3.14$. This means that one complete rotation of the disk is completed within a timeframe of t=6.28s. For all runs, a fixed time-step is used, such that the Courant number can be kept at around 0.05. Two different grid sizes are used, one coarse (64x64cells) and one fine (128x128). In the cases where dynamic local refinement is used, the basis coarse grid is chosen to be 32x32cells, which when refined one and twice respectively fits the accuracy of the aforementioned grid sizes (inside the refined space). The distance from the interface, where the grid is locally refined, is chosen as $D_o/6$.
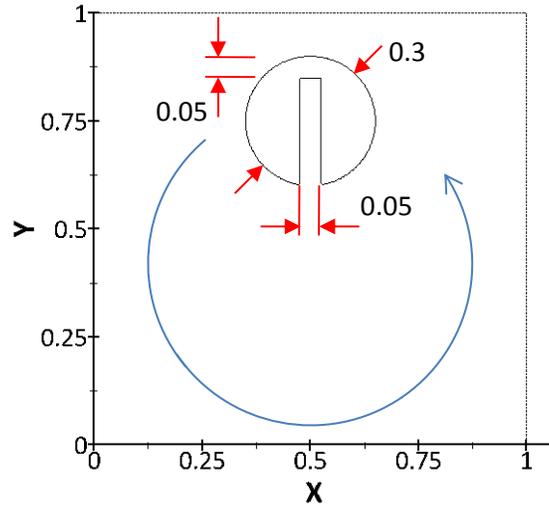

Figure 4. Initial domain and dimensions for Zalesak's disk benchmark Case.

The goal of this benchmark case is to successfully rotate the disk without any deformation. This is a typical advection test for two-phase flows, where the accuracy of the advection algorithm is tested in much coarser grids than the ones usually used for real conditions runs (especially for interface tracking runs). However, in this study, the advection accuracy is not the main goal. The crucial goal is to use the sharpening equation for the smallest disk deformation to be achieved, in respect to the advection algorithm.

Results of the iso-value of $\alpha=0.5$ after one revolution of the disk are presented in Figure 5 for the two grid sizes (64x64, 128x128) plus for another one (32x32), which is refined twice so as to resemble the grid density of the fine grid. In the first row (of Figure 5), the numerical results for the default discretization schemes of CICSAM and HRIC are presented. It is clear that the advection is not absolutely perfect for both schemes, even for the fine grid, while the use of dynamic local refinement has a slight effect on the disk shape in the form of small visible wrinkles inside the slot.

In the second row of Figure 5, the effect of the sharpening scheme is presented. For the coarse grid, the disk after one revolution has changed into a 'donut' (shape). This is attributed to the way this sharpening equation (eq. 7) works. More specifically, the ε parameter which controls the interface thickness, at a value of Δx/2 will 'preserve' a thickness of approximately 3-4 cells unconditionally, meaning that the thickness is not affected by grid size. For that case, owed to the fact that the grid is coarse, when the sharpening equation is applied, the interface becomes slightly wider, and as a result the two parts of the slotted disk coalesce at the bottom into one and finally form a 'donut'. On the other hand, for the fine grid case, the effect of the sharpening scheme (presented in Figure 5) is minimal, especially for the case of HRIC+SHARP. Therefore, equation 7 does not affect considerably the solution

of the default HRIC, which is the main goal of this benchmark case. In other words, the coupling of the HRIC with the sharpening algorithm cannot be claimed to provide a more accurate solution in terms of liquid phase advection than the default HRIC and/or CICSAM, or alternatively that it provides a higher accuracy advection algorithm. Finally, the use of dynamic local grid refinement technique delivers almost the same results with the fine grid for the case of the proposed sharpening scheme.
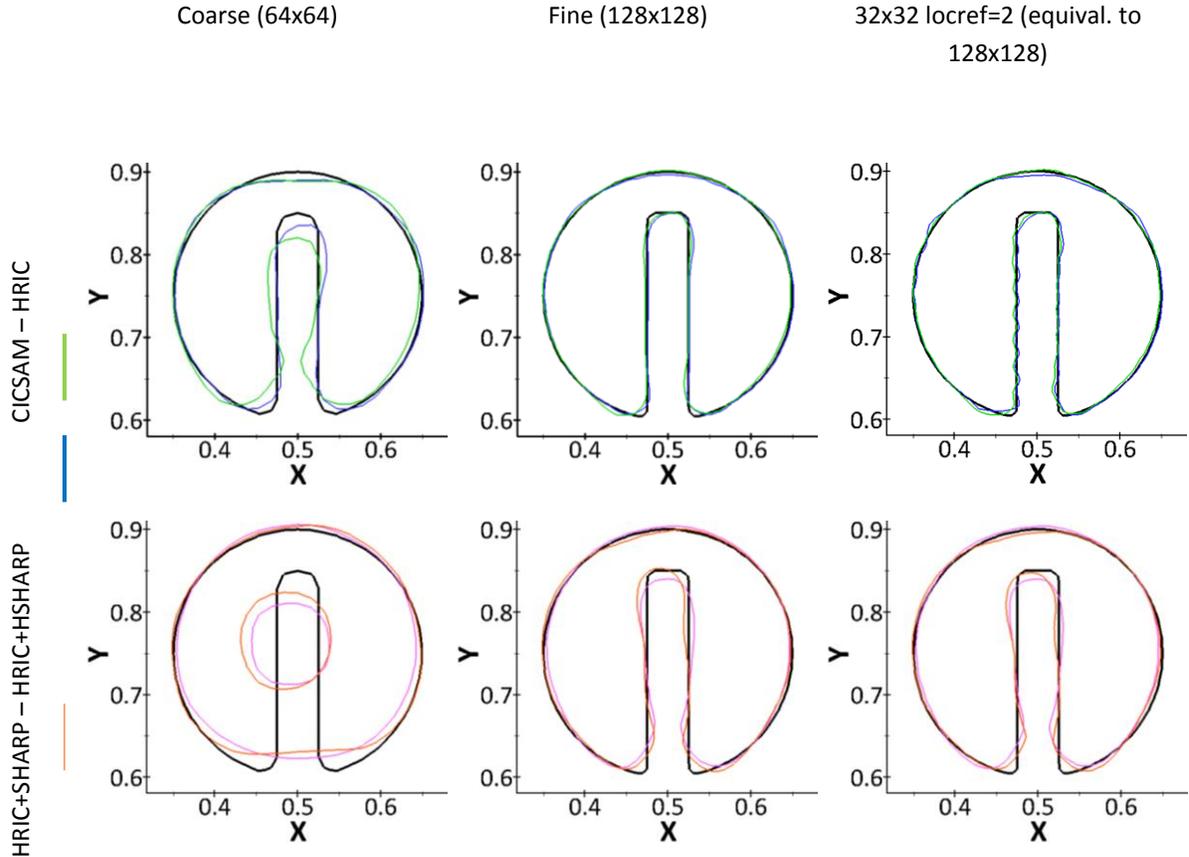

Figure 5. Zalesak's disk after one revolution. Isoline of α=0.5 is plotted, together with the reference shape.

3.1.2   Single Vortex in a deformation field

In this benchmark case which was first presented in the work of Rider and Kothe [53], an initially static circular fluid body, is again centered at (0.5, 0.75) in a rectangular domain and is subjected to a single vortex, which axis of rotation is located at the center of the domain. This vortex is described by the following stream function:

$$\Psi = \frac{1}{\pi}\sin^2(\pi x)\sin^2(\pi y) \tag{11}$$

and the derived velocity components are therefore found as:

$$u = -\frac{\partial \Psi}{\partial y} \ , \ v = \frac{\partial \Psi}{\partial x} \tag{12}$$

As a result, the circular fluid body stretches to form a 'fluid spiral'. The interface thicknesses of the deforming shape, as well as the numerical diffusion of values located at the tail of the fluid body during

its 'spiral motion' are of importance. The initial domain dimensions for this benchmark case are presented in Figure 6a. Figure 6b presents the exact solution at a time instant of t=2.5s (stated here as the reference time), and is derived by the motion of 10^4 massless particles placed at the interface of the circular fluid body following a Lagrangian approach.

a.   **b.**
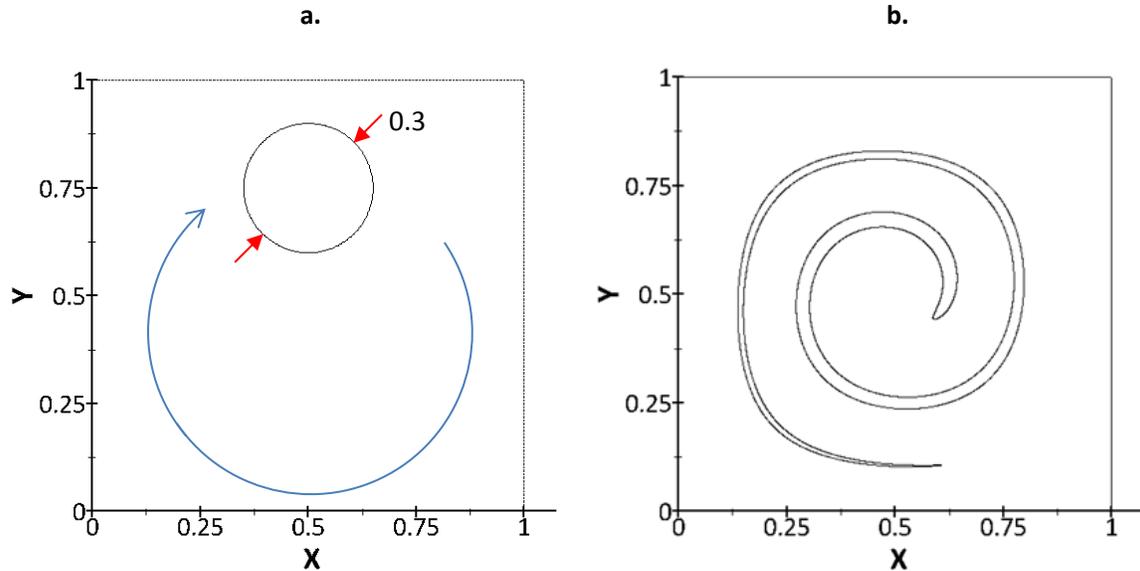

Figure 6. Initial domain and dimensions for Single Vortex benchmark Case and exact solution at t=2.5.

This case is as well simulated with parameters being the same as the ones mentioned in the previous case, i.e. a) four different algorithms, namely CICSAM, HRIC, HRIC+SHARP, HRIC+HSHARP on b) three different grid sizes, coarse (64x64), fine (128x128) and a coarser one (32x32) using 2 levels of local refinement. Again a fixed time-step is used, corresponding to a Courant number of 0.2, while all runs are performed until an absolute time of 6 sec.

For a direct comparison of the different methods, the reference time instant of t=2.5s is chosen for depiction. Figure 7 presents the numerical results of all runs at t=2.5s.
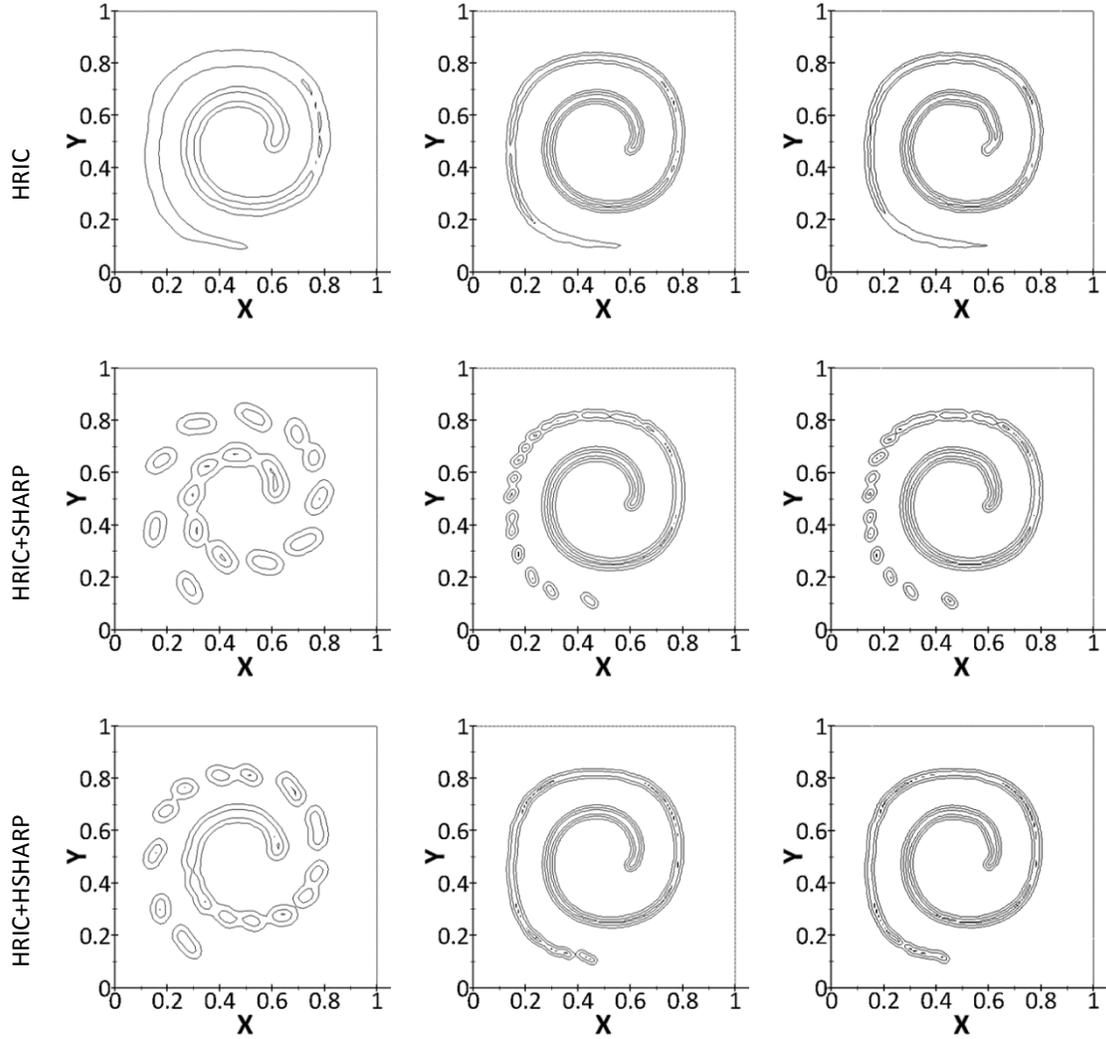
Coarse (64x64)   Fine (128x128)   32x32 locref=2 (equiv. to 128x128)
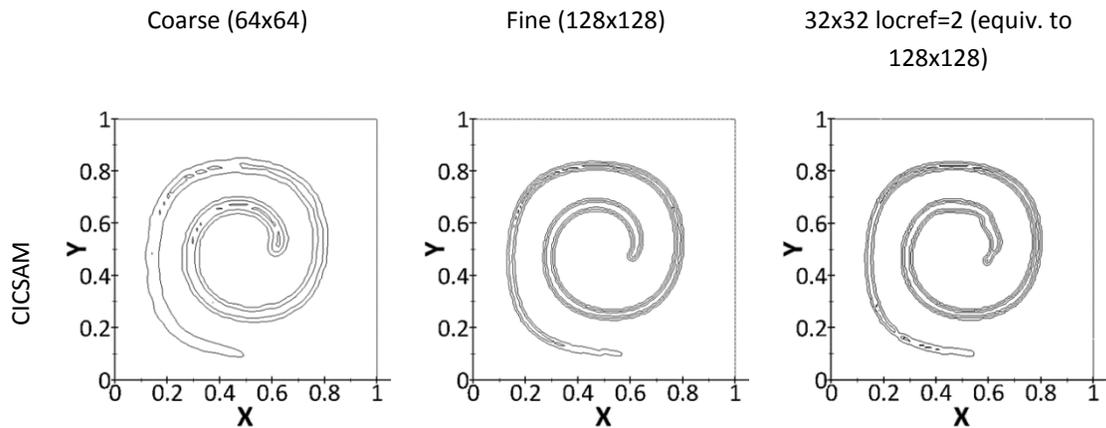
Figure 7. Single Vortex Case at t=2.5. Isolines of α=0.1, 0.5, 0.9 are plotted.

For the coarse grid, it is obvious that in terms of diffusion CICSAM behaves in the best way compared to all other schemes. HRIC is the more diffusive as expected, while enhancing HRIC with any sharpening algorithm in a coarse grid results in the liquid mass fragmentation. While this is not the favorable result, it seems inevitable to avoid such a fragmentation for any applied sharpening algorithm (also seen in Sato and Niceno [34]), especially at regions where the liquid body becomes very thin. The explanation lies on the fact that the redistribution of volume fraction values (after the application of the sharpening equation) is performed along the interface normal direction (vector $\hat{n}$). Consequently, the fluid body is thinning in a more intensive way than the conventional discretization schemes apply and finally the two sides of this thin liquid mass are solely represented by one or two maximum cells. As a result, inevitably the liquid splits and under the influence of surface tension force small liquid satellite "droplets" are formed.

In the fine grid case, the application of HRIC with a sharpening step results in a slight deformation of the liquid body, which however tail is now sharper than the corresponding derived with CICSAM. HRIC with the default sharpening scheme (HRIC+SHARP) does not seem to improve the numerical results compared to the default HRIC. Nevertheless, it is very important to point out that in Figure 7 a constant interface thickness along the full length of the liquid mass is achieved (HRIC+SHARP). On the other hand, the

application of HRIC with HSHARP improves significantly the derived results compared to HRIC (the isolines are closer together), in terms of diffusion, whilst compared to CICSAM the tail of the fluid body is not diffused. Finally, for all cases examined, concerning this benchmark case, the application of the dynamic local refinement technique does not affect the solution considerably, except for the cases of CICSAM and HRIC, where severe liquid body deformation is observed on its front face. It should be pointed out that this benchmark case aimed at investigating what effect the coupling of standard HRIC with a sharpening algorithm would have on the transport of the deforming liquid mass. This methodology was proven to suppress diffusion, when compared to the corresponding one of the standard HRIC scheme.

Based on the results of all aforementioned benchmark cases, it can be concluded that the proposed coupled algorithm does not improve colour function advection, but improves significantly its diffusion behavior.

Except from the theoretical cases examined, this study provides results concerning the proposed algorithm for real cases as the one of droplet acceleration under the influence of gravity for low Weber and Reynolds numbers and droplet impingement onto substrates, when interacting with a gaseous environment.

3.2   Gravitational Acceleration of a freefalling water droplet

3.2.1   Case Description – Analytical Solution

The simulation of a water droplet executing a freefall is very important for the validation of any algorithm of two-phase flow. The correct prediction of the surface tension force and how this is applied in a computational domain is a measure of how accurately any interface tracking model behaves. In order to magnify the arithmetic difficulties imposed by such issues, the fluids chosen are water and air. In that way, due to large density ratio, the discontinuity (jump conditions) at the interface is quite large, making the correct application of forces more trivial and sensitive to small changes. Moreover, the size of the droplet is chosen to be very small (D_0 = 0.5mm) thus implying quite high induced surface tension forces. In the book of Clift [54], the predicted shape of such a small droplet on freefall appears to be almost spherical (for Eotvos number = 3.35E-02, log(Morton) = -11.76 on Figure 2.5 on Clift book [54], Table 1).

The dimensionless numbers that govern the phenomenon are the Eotvos, Morton and the Reynolds numbers.

The analytical solution that is used for the validation of the CFD model is derived from solving a simple 1-D balance of forces acting on the droplet. The equation of motion for a droplet on freefall is described by the balance of droplet weight with the drag force induced by air surrounding the droplet, minding as well for the buoyancy of the displaced air:

$$m\vec{a} = \Sigma F = F_{\vec{g}} - F_d \implies \rho_{liq} V_{liq} \frac{du}{dt} = \rho_{liq} V_{liq} g - \rho_{gas} V_{liq} \vec{g} - c_d \frac{1}{2} \rho_{gas} u^2 A_{liq} \implies \tag{13}$$

$$\frac{du}{dt} = -c_d \frac{1}{2} \frac{\rho_{gas}}{\rho_{liq}} \frac{A_{liq}}{V_{liq}} u^2 + \left(1 - \frac{\rho_{gas}}{\rho_{liq}}\right) \vec{g} \tag{14}$$

The simple 1-D balance of forces results in equation 14, where the ratio of A_{liq}/V_{liq} is equal to $3/2D_o$ for a spherical droplet. Drag coefficient is calculated from the correlations given in Table 5.2 of Clift book[54]. Equation 14 is solved implicitly taking as initial condition, a zero droplet velocity. The stopping criterion is defined by when the droplet reaches its terminal velocity, i.e. when u_{new}-u_{old} < small number (in this case

set equal to 1E-05). In Table 1 the initial conditions used for the solution of equation 14 are presented. After solving this equation, the terminal velocity is calculated as being 2.006m/s, which agrees quite well with Fig. 5.14 of Clift book [54] (graph presenting terminal velocities of spheres in air and water). Therefore the temporal evolution of the droplet velocity, found by solving this equation, can be used for the validation of the proposed algorithmic model.

Results of the analytical solution for a water droplet taking a freefall on air are presented in Table 1, while the temporal evolution of velocity and displacement of droplet are shown in Figure 8.

Initial Conditions				Results	
D_o	0.5mm	μ_{air}	1E-05 kg/ms	$u_{terminal}$	2.006 m/s
u_o	0m/s	M_o	1.7894E-12	t	703.8 ms
ρ_{liq}	1000 kg/m^3	E_o	3.35E-02	X/D_o	2187.7
ρ_{air}	1.225 kg/m^3	Δt	1E-05	Re_{gas}	68
μ_{liq}	0.001003 kg/ms			We	26.97

Table 1. Initial Conditions and Results of the 1-D analytical solution of a water droplet on freefall.

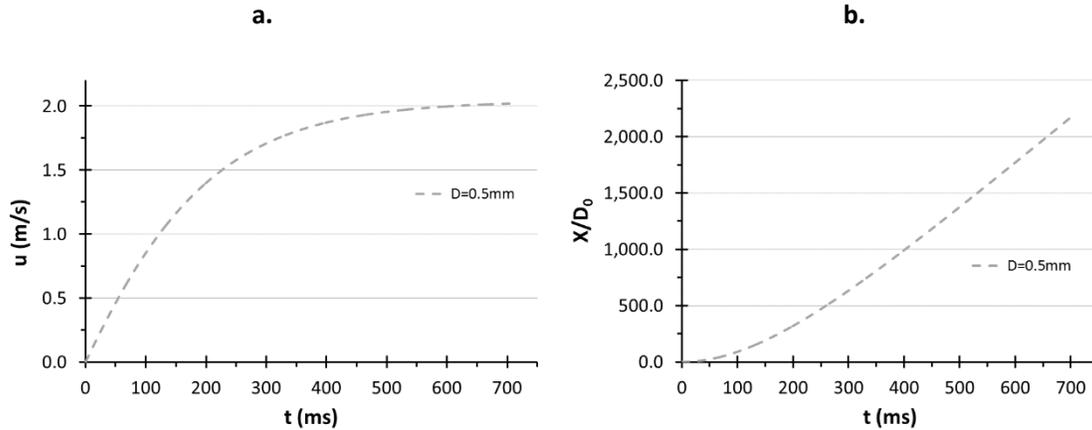a.   b.

Figure 8. Temporal evolution of a) velocity and b) displacement of a single droplet accelerated by gravity. Results of the 1-D analytical solution.

3.2.2   Initial Domain – Boundary Conditions

Due to the large displacement of the droplet (almost 2200 times its diameter), the computational grid needs to be many times larger than the droplet diameter, resulting in extravagant number of computational cells which cannot be accomplished, capturing a high level of accuracy. For that reason, a moving numerical grid along the droplet mass center velocity is applied for that simulation. The velocity of the grid is updated in the beginning of every time-step and equals the mass averaged velocity of the droplet, i.e.

$$u_{grid} = u_{droplet} = \frac{\sum_{cell} u_{cell} m_{cell}}{\sum_{cell} m_{cell}} = \frac{\sum_{cell} u_{cell} \alpha_{cell} \rho_{liq} V_{cell}}{\sum_{cell} \alpha_{cell} \rho_{liq} V_{cell}} = \frac{\sum_{cell} u_{cell} \alpha_{cell} V_{cell}}{\sum_{cell} \alpha_{cell} V_{cell}} \qquad (15)$$

, where u, α,V are the cell axial velocity, volume fraction and Volume values respectively.

The droplet is initially placed in the center of the axis on a grid (100x50 cells) with dimensions $20D_o$ x $10D_o$ (0.01m x 0.005m), as depicted in Figure 9 together with the boundary conditions. Dynamic local grid refinement technique is used, where the densest region extends to a distance of $D_o/6$ from the interface (Figure 9b). The time-step which is used is either fixed or variable aiming always to have a constant Courant number equal to around 0.25.
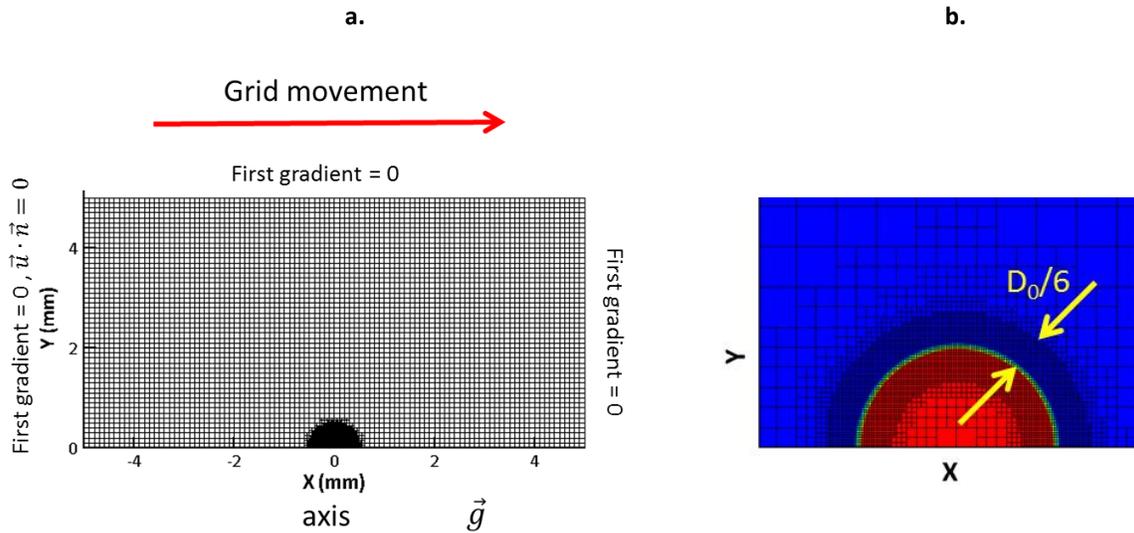

Figure 9. a) Initial Domain + Boundary conditions for the gravity Case. b) Dynamic Local Refinement Technique

3.2.3   Simulated Cases

Overall, 15 Cases are investigated, similar to the ones afore-presented (CICSAM, HRIC, HRIC+SHARP, HRIC+HSHARP). However, this time three different grid sizes are used, based on the maximum levels of local refinement which are applied. In the first 14 Cases, the droplet starts from zero velocity, and this should show the ability of the model to overcome spurious velocities formed during the beginning of the acceleration progress. The first 12 Cases are run for only 200ms using a fixed timestep owed to the large computational time required for the full description of the phenomenon, i.e. 700ms. The computational time is as well limited to the 2/7 of the whole time as the main purpose of this investigation lies on the examination of the acceleration phase from a zero velocity field and how this is evolving. In Cases 13-14, the end time of the simulation is set to 700ms, approximately the time when the 0.5mm droplet reaches its terminal velocity, while the time-step used is variable always keeping a Courant number approximately equal to 0.25.

Case No.	a/a with parameters distinction	U_0 (m/s)	Refin. Levels	Cells in R	End time (sec)	Time – step (Δt)	Courant (max)	Method
1	1a	0	**4**	**40**	0.2	2E-06	0.48	**CICSAM**
2	1b	0	**5**	**80**	0.2	1E-06	0.48	CICSAM
3	1c	0	**6**	**160**	0.2	5E-07	0.48	CICSAM
4	2a	0	4	40	0.2	2E-06	0.48	**HRIC**
5	2b	0	5	80	0.2	1E-06	0.48	HRIC
6	2c	0	6	160	0.2	5E-07	0.48	HRIC
7	3a	0	4	40	0.2	2E-06	0.48	**HRIC+SHARP**
8	3b	0	5	80	0.2	1E-06	0.48	HRIC+ SHARP
9	3c	0	6	160	0.2	5E-07	0.48	HRIC+ SHARP
10	4a	0	4	40	0.2	2E-06	0.48	**HRIC+HSHARP**
11	4b	0	5	80	0.2	1E-06	0.48	HRIC+HSHARP
12	4c	0	6	160	0.2	5E-07	0.48	HRIC+HSHARP
13	5	**0**	**4**	**40**	**0.7**	Var.	0.25	**HRIC+ SHARP**
14	6	**0**	**4**	**40**	**0.7**	Var.	0.25	**HRIC+ HSHARP**
15	7	**1.5**	**6**	**252**	**0.005**	Var.	0.25	**HRIC+HSHARP**

Table 2. Test Cases Investigated for a 0.5mm droplet on freefall.

For the latter Cases 13-14 it is important to notice that the steady internal recirculation inside the liquid droplet is predicted in accordance with theoretical analysis, along with the slow droplet acceleration until the drag force equals the droplet mass weight and its velocity remains approximately constant. Finally the last case examined (Case 7) is run only for 5ms of simulation time in order to validate the induced droplet internal circulation using an initial velocity condition of 1.5m/s ($\approx 0.75*u_{terminal}$), at a smaller domain ($10D_o$ x $5D_o$) and a smaller refinement region ($D_0/30$) compared to the rest, which however has the highest grid density. The properties of all investigated cases is presented in Table 2.

The coarse mesh has grid spacing such that one droplet radius is discretized by 5 cells (0.005m/100cells). In this way, when dynamic local refinement is applied, the minimum cell size changes to $\Delta x_{initial}/2^{level}$ since at each level all parent faces are split in two children (axisymmetric case) ones. Therefore, each droplet radius is covered by $5*2^{level}$ cells. The value of 160 cells discretizing a droplet radius presented in Cases 3,

6, 9 and 12 is in accordance with the current state-of-the art maximum grid resolutions applied for such cases.

Table 3 presents the number of cells required either using the proposed local grid refinement technique or an equivalent uniform grid, to achieve the same droplet discretization. From the values presented, it is obvious that the use of local refinement can decrease the number of computational cells by almost three orders of magnitude while having the same grid resolution at the droplet interface for the cases examined (4, 5 and 6 levels of local refinement). For reasons of completeness, it was decided to run the case of droplet acceleration under the effect of gravity for a cell size equal to $D_o/20$ (1 level of local refinement) using both local grid refinement and an equivalent uniform one. The results presented in Appendix B, prove that the numerical accuracy is almost the same with a decrease of associated computational resources by around 400%.

Levels of Refinement	#cells using local refinement	#cells of an equivalent uniform grid
1	5,180	20,000
2	5,888	80,000
3	6,998	320,000
4	9,086	1,280,000
5	13,238	5,120,000
6	21,728	20,480,000

Table 3. Number of initial cells for a grid where the local refinement is used and another equivalent in resolution, but with uniform refinement.

3.2.4   Results of the simulation

In Figure 10a,b, the corresponding picture of Figure 1 is shown for the prediction of the numerical diffusion using CICSAM alone and HRIC after the application of the proposed sharpening scheme, which counterbalances the high diffusion of volume fraction. Figure 10c presents the induced velocity field as derived by the application of CICSAM at the interface, demonstrating the unphysical direction of the velocity vectors imposed indirectly (owed to high and to a certain extent unphysical curvature values) by its strong non-diffusive character, in accordance with what is mentioned in the Introduction Section. On the other hand, Figure 10d, presents the corresponding velocity vectors as derived by the application of HRIC, which is smoother and more reasonable compared to the previous one. Both vector fields are plotted in the same manner (using as a reference vector a value of 0.2 Grid Units/Velocity Magnitude). The underlying numerical reason for this to happening lies on the fact that CICSAM impose greater surface tension forces at the interface, owed to high VOF gradient values, which in turn affect in a negative way the induced velocity field as calculated by the governing momentum equation (higher velocity values together with vector turn).

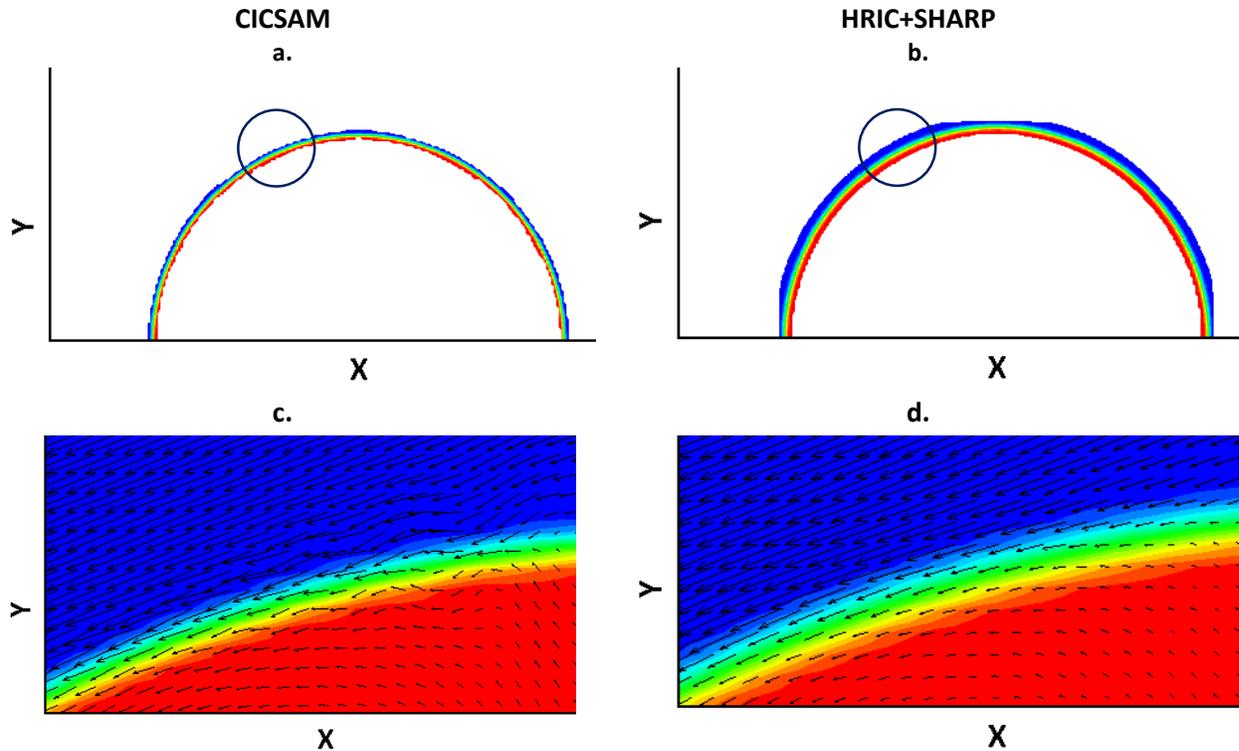**CICSAM**
a.

HRIC+SHARP
b.

c.

d.

Figure 10. Comparison between (a,c) CICSAM and (b,d) HRIC+SHARP for predicting the relative velocity of a droplet after 30ms for Cases 1a and 3a, as well as the volume fraction field. Volume fraction values between 0.001 and 0.999 are shown. Velocity vectors are plotted in the same manner for the two Cases (using the value of 0.2 Gird Units/Velocity Magnitude).

It now becomes clear that using HRIC discretization scheme together with the sharpening equation 7, is beneficial, a) not only for the absolute velocity magnitude which is now more uniform across the interface, but also b) for the volume fraction field as this can be limited (suppressed) to a specific constant thickness (imposed by the selected value of ε). It is also clear that the new interface thickness calculated by HRIC+equation7 is always larger than the corresponding using the CICSAM discretization scheme, but its basic advantage is the smooth transition of volume fraction values, allowing for the calculation of smoother VOF gradients, which in turn are reflected to a smoother curvature profile and hence surface tension force. Additionally, the use of High Sharpening (HSHARP) results in a constant interface of smaller thickness than what the SHARP predicts, Figure 10.

Figure 11 presents the numerical results for the temporal evolution of mass averaged droplet velocity and its axial transport for all different methods proposed (Cases 1-4) against the 1-D analytical solution for the first 200ms of the phenomenon. Additionally, the effect of grid density on the numerical results is presented.
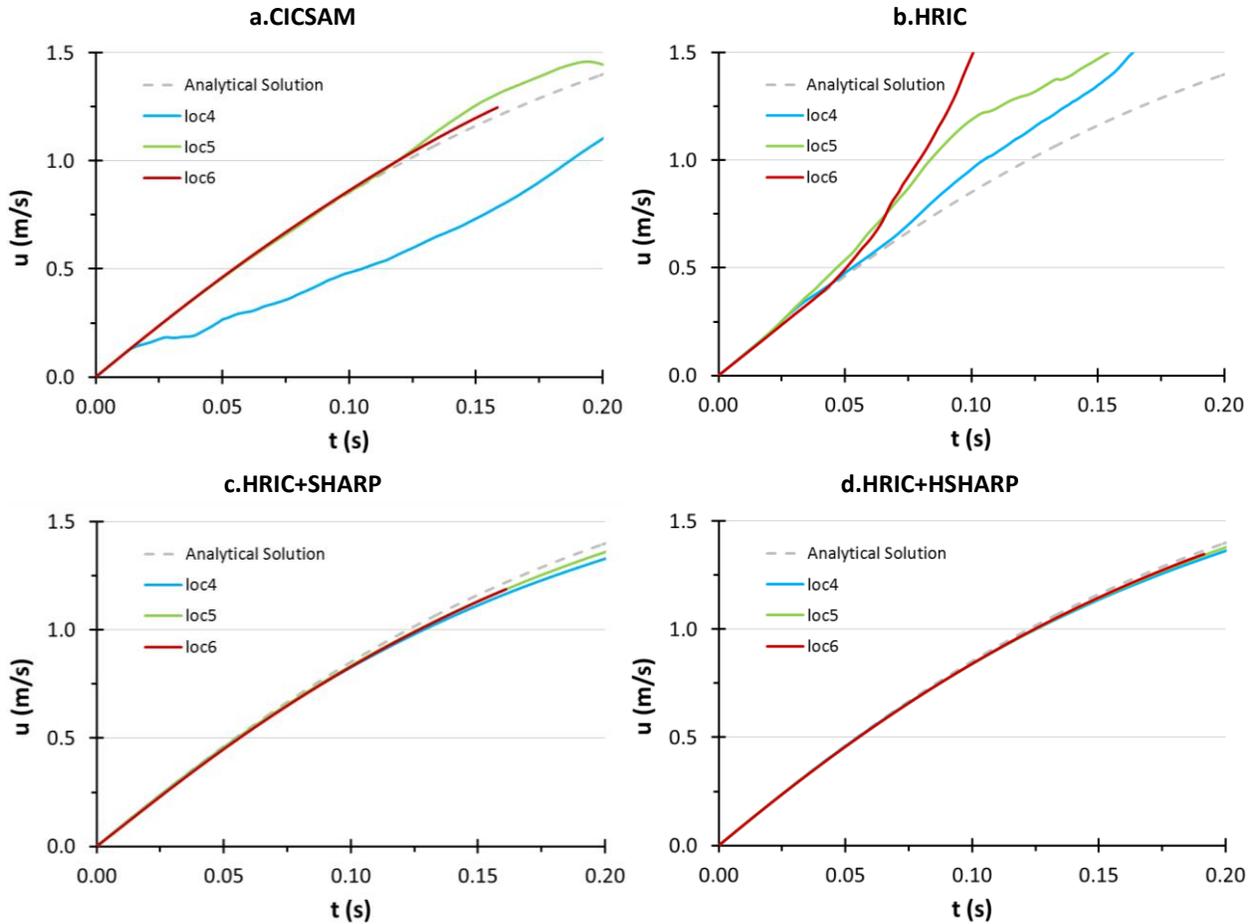
Figure 11. Temporal evolution of droplet velocity as calculated from CFD compared with the 1-D analytical solution. Cases 1-4

Figure 11a and b, present the comparison of droplet velocity temporal evolution against the analytical solution using the standard CICSAM and HRIC schemes. The deviation that is observed in the prediction of droplet velocity can be attributed to the diffusion of volume fraction. Even using a grid density of 40 cells per radius and CICSAM discretization scheme in Case 3 (Case 1c), after 200ms of run, diffusion of volume fraction is observed, Figure 12.
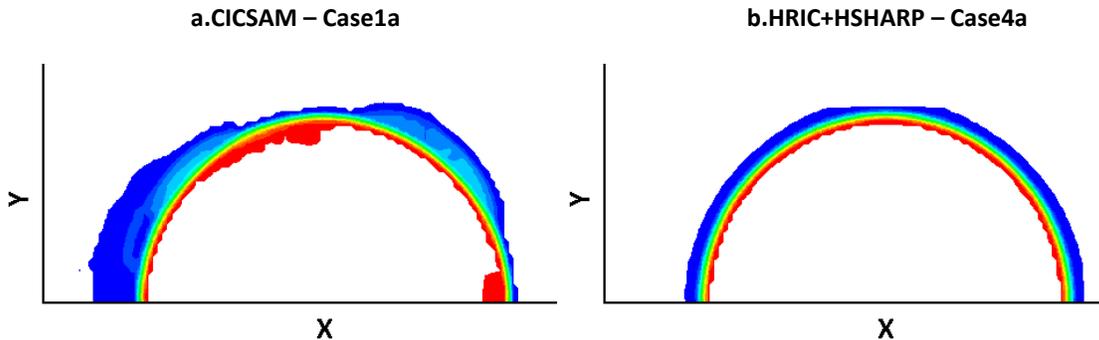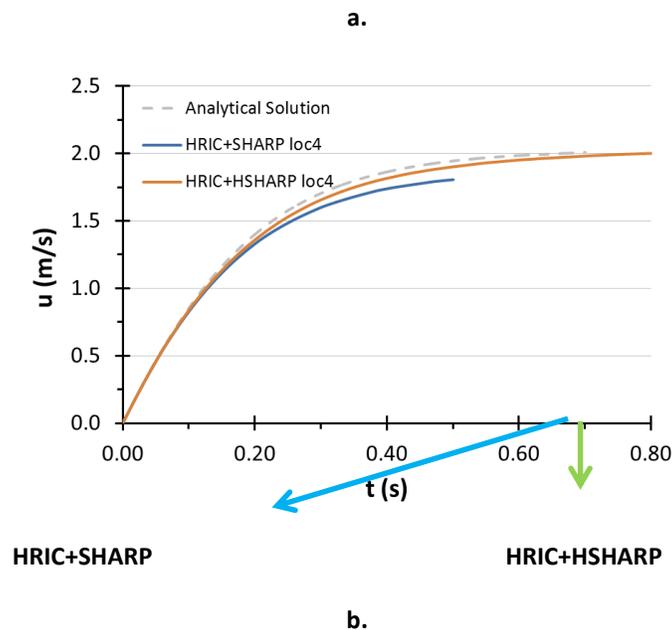

Figure 12. Comparison between a) CICSAM and b) HRIC+HSHARP for predicting the volume fraction field. Volume fraction values between 0.001 and 0.999 are shown.

This clearly states that for such a demanding case, a sharpening scheme is required for the Eulerian interface tracking algorithms applied here. Additionally, it is clear that the combination of HRIC with any sharpening equation delivers much better not only in terms of interface diffusion but also results in more accurate velocity field in the vicinity of droplet interface and macroscopically droplet average velocity, Figure 11c and d. In the case of HighSharpening (HSHARP), the results of the simulation are even closer to the 1-D analytical solution. The computed surface tension force seems to be more accurate in the case of HRIC+HSHARP, since the interface thickness is smaller and the transition from gas to liquid phase is steeper.

In order to shed light to the whole evolution of the phenomenon (t=700ms), Cases 13 and 14 have been as well examined, for which compared to the rest a variable Courant is used. Figure 13 presents the corresponding numerical results against the analytical solution of the 1-D model, while a minimum number of refinement levels equal to four (4) is selected for these runs so that the actual computational time can be kept as minimum as possible. Again the numerical results as far as the droplet acceleration temporal evolution is concerned are very promising, while Figure 13 presents as well the relative velocity streamlines (Relative Velocity = Mesh Velocity-Droplet Velocity) both of gas and liquid phases.

Based on the results of all cases examined, those produced by the implementation of HRIC either with the SHARP or with the HSHARP sharpening technique approach in the best way the 1-D analytical solution results, as mentioned before (steeper jump conditions). For both of these cases the internal liquid circulation induced by the motion of droplet is fluctuating between droplet front and rear face (streamlines in Figure 13). The recirculation behind the droplet is well predicted, while its dimension match the ones given by Feng and Michaelides [55] (missing exact number). Overall HRIC+HSHARP delivers the best results, with a total of 1.36% relative error in terminal velocity prediction (in 700ms), which for the specific grid density (40 cells in Radius) is considered to be as a satisfactory solution.
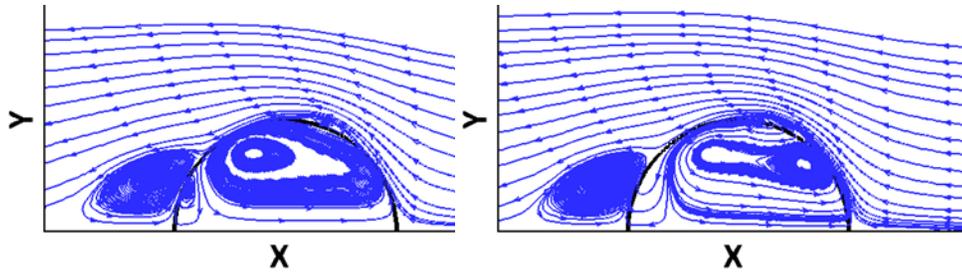
a.

b.

The aforementioned unphysical fluctuating behavior of the streamlines is mainly attributed to the induction of a small recirculation zone on the top right of the droplet, which even in the vicinity of such dense grid densities is grid dependent. Figure 14 presents the numerical results as derived by the application of Cases 10, 11 and 12 (Cases 4a,b,c using 40, 80 and 160 cells in radius). In that cases HRIC with HSHARP algorithm is implemented using three different dense grids, which unfortunately are not sufficient enough to capture in an efficient way the boundary layer formed on the top of the droplet. Feng and Michaelides [55] mention that a grid density of 500 cells in droplet radius is enough to resolve with accuracy this formed boundary layer showing that the streamlines are 'hugging' the droplet. Therefore given the numerical grid densities we use, the predicted "jump" of streamlines on the top right of the droplet can be probably considered as artificial and resembles that of a flow separation over an airfoil.
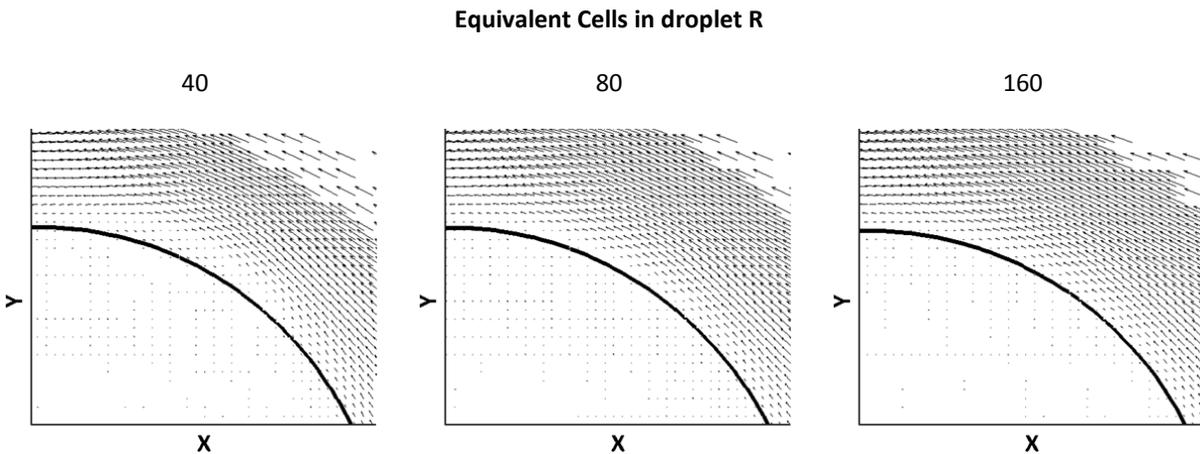
Equivalent Cells in droplet R

| 40 | 80 | 160 |

In that light and in order to catch the correct internal recirculation shape, the grid density was decided to be further increased reaching a value of 252 cells in Radius. This condition is presented as Case 15 and to save time the initial droplet velocity is assumed to be equal to 1.5 m/s (approxim. 75% of terminal velocity). Figure 15 presents the corresponding numerical results against a sketch originating from the book of Clift and Grace [54]. This sketch depicts the streamlines and vorticity contours when a raindrop of 0.6mm diameter has reached its terminal velocity, at a Reynolds number of 100. These conditions are very close to the ones used in this study. The direct comparison of the numerical results concerning the internal recirculation and vorticity, against the features of this picture is considered to be well acceoted. The numerical results are taken after 5ms of actual droplet acceleration. Under such a grid density the induced liquid streamlines are not fluctuating, giving rise to the claim that the under-resolution of the

boundary layer is responsible for the streamline non physical behavior shown in Figure 13. The recirculation center is nicely located towards the front end of the droplet, instead of its rear (Figure 13). Vorticity magnitude is also presented in Figure 15 using isolines on the left side of the droplet. Its difference with the sketch can be attributed to two reasons, first that the two cases do not have the same exact terminal velocity and secondly the grid density in the gas phase is probably much lower than the required one. Finally, the pressure coefficient which is also shown in the Figure, as a filled contour, is non-dimensionalized with the terminal velocity as:
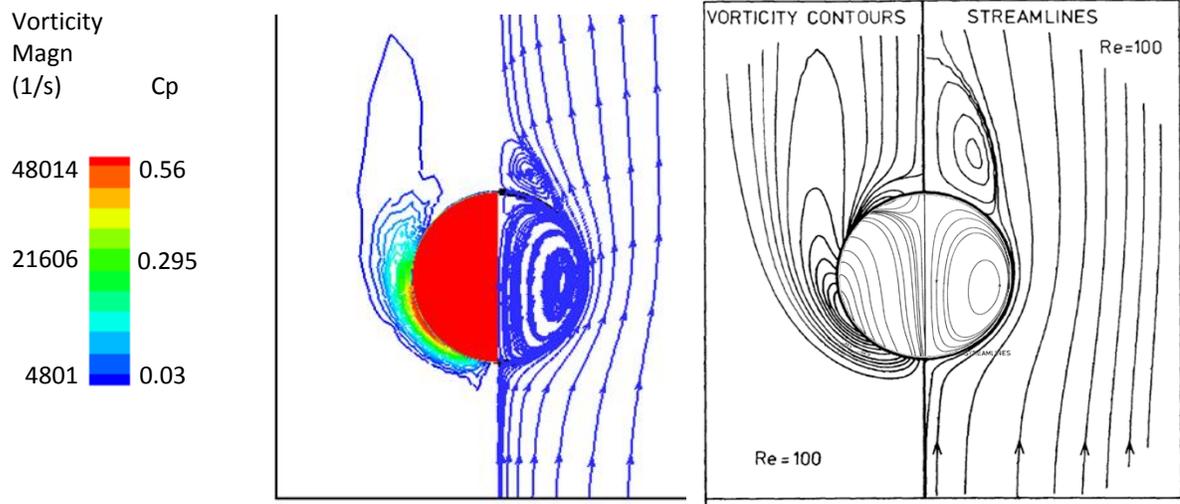
$$C_p = \frac{P}{1/2 \rho_{liq} u_{term}^2}$$

(16)

Figure 15. Comparison of internal (liquid) and external (gas) recirculation. Simulation results obtained after 5ms of run with u=0.75*u$_{terminal}$ initialization. Image on the right taken from Clift [54] (Figures5.26-5.27, D=0.6mm, Re=100, terminal velocity).

3.3 Water droplet impingement on a solid flat surface

3.3.1 Case Description – Initial Domain

The proposed numerical algorithm is as well tested for the case of a water droplet impinging onto a solid flat hydrophilic surface at high Weber number. This case is experimentally investigated by Fukai et al. [8] and is chosen because it contains all three most characteristic phases, a spreading droplet exhibits when interacting with a solid substrate, namely the spreading, recoiling and relaxation phases. Moreover, the boundary condition of the prescribed contact angle value at the sharpening equation 7 will be discussed. Properties for this case are presented in Table 4

Case No.	U$_0$ (m/s)	D0 (m)	θadv – θrec	We	Refin. Levels	Cells in R	Time – step (Δt)	Courant (max)	Method
1	1.5	3.76e-03	60 - 22	112	3	50	Var.	0.25	CICSAM
2	1.5	3.76e-03	60 - 22	112	3	50	Var.	0.25	HRIC

3	1.5	3.76e-03	60 - 22	112	3	50	Var.	0.25	**HRIC+ SHARP**
4	1.5	3.76e-03	60 - 22	112	3	50	Var.	0.25	**HRIC+HSHARP**
5	1.5	3.76e-03	60 - 22	112	**4**	**100**	Var.	0.25	**HRIC+SHARP**

Table 4. Test Case Investigated for a water droplet impinging on a solid flat hydrophilic surface.

The initial axisymmetric domain, which is used for the simulations, is presented in Figure 16a. The coarse grid comprises of 60x60 identical quadrilateral cells, while the spatial coordinates of the grid range between $X,Y = 0 \div 0.015m$ (x- axial coordinate, y-radial coordinate). The droplet is initially placed at a distance of one equivalent droplet diameter, so that the gas fluid flow around the droplet can develop in a physical way, just before it impinges onto the surface. In Figure 16b, a zoomed area of the applied dynamic grid around the moving droplet is shown, as well as the initial droplet position, the specific distance of refinement and droplet velocity, U_o .
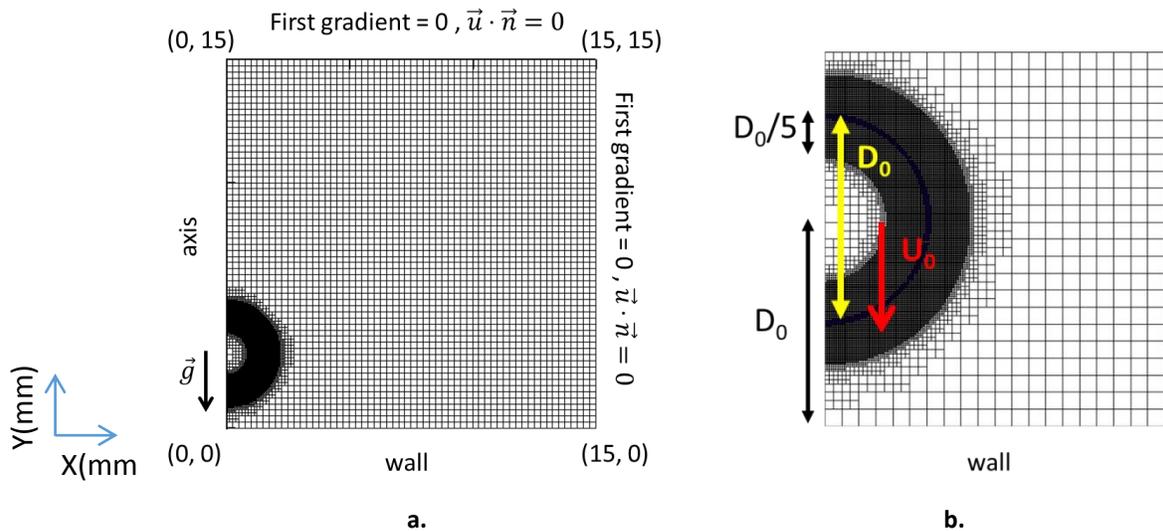

Figure 16. a) Initial Domain + Boundary conditions for all cases, b) Depiction of the local refinement technique, c) calculation of θdyn for the WFM.

3.3.2   Results of the simulation

All the results for different setups examined, are presented in Figure 17, where the temporal evolution of droplet spreading along with time of the phenomenon is shown. Overall, the numerical results indicate that the use of boundary condition in the sharpening scheme in order to account for the imposed contact angle as explained in Section 2.2 delivers good results, as the temporal evolution of the phenomenon is captured well, in comparison with the CICSAM case, at least for the initial stage of the phenomenon. At this point CICSAM scheme acts as a reference point due to its very sharp interface capabilities. During the recoiling phase of droplet spreading, however, and owed to the very low contact angle the liquid phase exhibits at its rim, the height of liquid rim cannot be resolved by the accuracy of the coarse mesh. This is illustrated in Figure 17a,b, where the depicted slight 'jump' of dimensionless spreading ratio (Case 3) during the recoiling phase is attributed to the breakup of the liquid film (Figure 17b), further decelerating the droplet retracting motion.
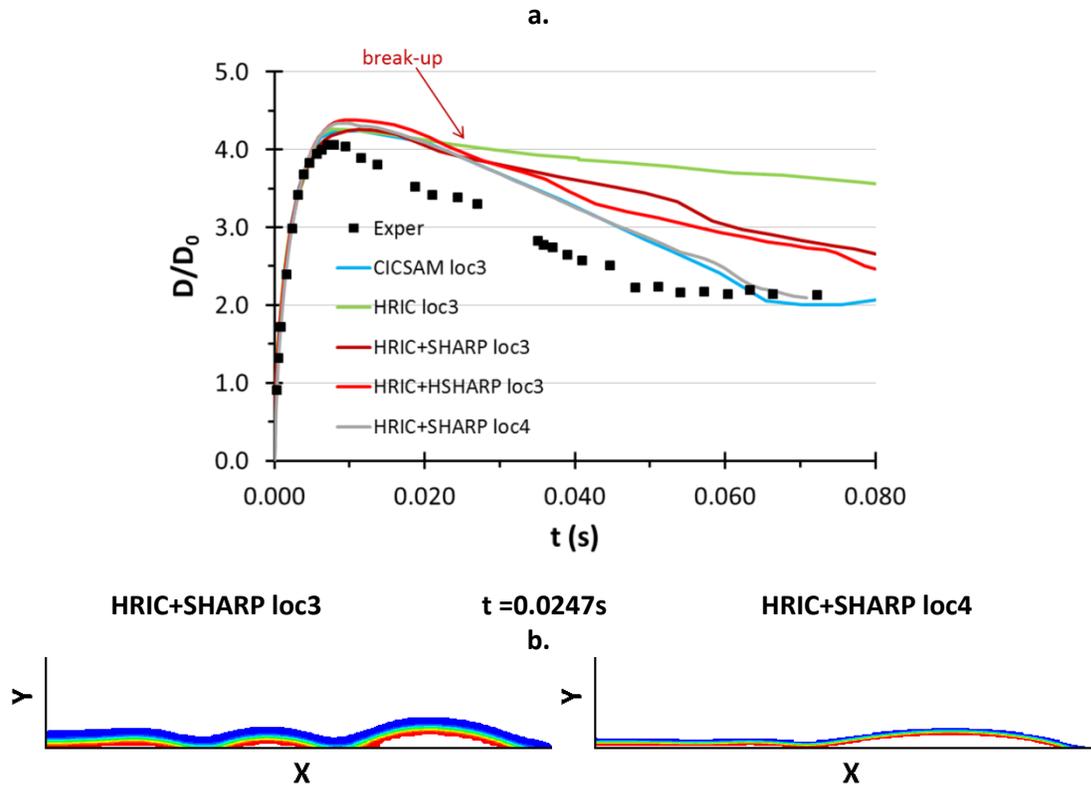
Figure 17. Droplet spreading diameter plotted against time for the Cases presented in Table 4.

When refining the grid (up to cpR=100, Cases 3,5), the liquid film thickness is now resolved and the results of the simulation resemble the ones after the use of CICSAM discretization scheme. It is clear that the implementation of the sharpening algorithm does not affect the flow field solution, while the volume fraction field is well conserved. Nevertheless, in the extreme case of the very low contact angle as presented in this study, the proposed sharpening scheme offers quite thicker interface which needs to be resolved by the computational grid and is the main reason for the deviation observed in the recoiling phase, especially when compared with CICSAM case.

The standard HRIC case exhibited diffusion problems, as outlined in this study. However, again, the use of the sharpening algorithm suppressed successfully the numerical diffusion.

It is thus concluded that both for this case, as well as for the droplet motion on free-fall, the implementation of the sharpening equation to the VOF model can promote the use of coarse grids (cpR<= 50). However, the accurate prediction of flow parameters, which are of smaller scale, such as the prediction of internal recirculation during droplet motion, and thus the correct prediction of drag coefficient for droplet under free-fall conditions, or the exact liquid elongations that result in a very thin film would require a much finer grid in order to be resolved.

4. Conclusions

This study presents numerical results as derived by the implementation of an interface sharpening method, in the framework of standard VOF methodology, in order to one hand to suppress the numerical

diffusion of the volume fraction field and to additionally smooth the effect of surface tension force in the induced velocity field imposed during the deformation of liquid droplets flowing within a gas stream. The sharpening equation uses as an input the volume fraction field, as initially calculated by the standard VOF method and subsequently 'suppresses' it to a specified thickness. This algorithmic intervention allows for smoother transition from gas to liquid phase.

In this study, this correction equation is solved coupled with the momentum equation, where the 'uncorrected' volume fraction field is used as a basis for calculations. Subsequently, the 'correct' values at the end of each time-step patching is performed, in order to save computational resources. The application of this approach together with an adaptive local grid refinement technique can reduce significantly the actual time of simulations without loss of accuracy. In general, the application of this coupled algorithm has a positive effect on simulation results given that it achieves a constant interface thickness along with a more uniform distribution of volume fraction values at the interface than the standard VOF method does. This in turn results in better and smoother calculation of the surface tension forces.

This algorithm is at first level tested on two benchmark cases and then on the real case of a 0.5mm water droplet free falling in an open air field accelerated by gravity. The derived results indicate that the use of HRIC discretization scheme for the volume fraction advection when coupled with the proposed sharpening scheme can deliver better results compared to standard approaches, as the interface is both steeper and more uniform than the one foreseen in a stand-alone VOF methodology. Additionally, the prediction with high accuracy of the terminal velocity of a single droplet on a basis of a very coarse grid (using the HRIC+HSHARP algorithm) is a highlight of this study, compared to the CICSAM scheme, which over predicts droplet acceleration. In the second real case of droplet impingement onto a solid flat surface, the proposed algorithm tracks with the same accuracy the induced velocity and liquid fields, though the spreading rim is becoming very thin. It is therefore recommended in such cases, high density grid to be utilized. To sum up, the proposed scheme seems promising and though it cannot be claimed to provide more accurate solutions in terms of liquid phase advection, it can used in order to efficiently suppress color function diffusion. This approach should mostly be oriented for cases, where surface tension effects or pressure jump conditions are important, and is worth being studied in additional realistic conditions such as droplet impingement onto solid surfaces coupled with phase change phenomena.

Acknowledgements

Appendix A.   Geo-Reconstruct predictions in the case of Zalesak's disk and drop acceleration

The performance of Geo-Reconstruct was evaluated as a discretization scheme for its use on the current study numerical tests. Based on the work of [56], where all provided FLUENT advection schemes are tested in terms of the induced spurious currents for a benchmark case (Static Droplet in a Quiescent Fluid), it is shown that the application of Geo-Reconstruct results in the highest value of spurious currents. Therefore, the choice of CICSAM seems to be a more reasonable choice. Moving forward, in Figure 18, the results of

the two "non-diffusive" discretization schemes CICSAM and Geo-Reconstruct are presented for the Benchmark case of Zalesak's disk.
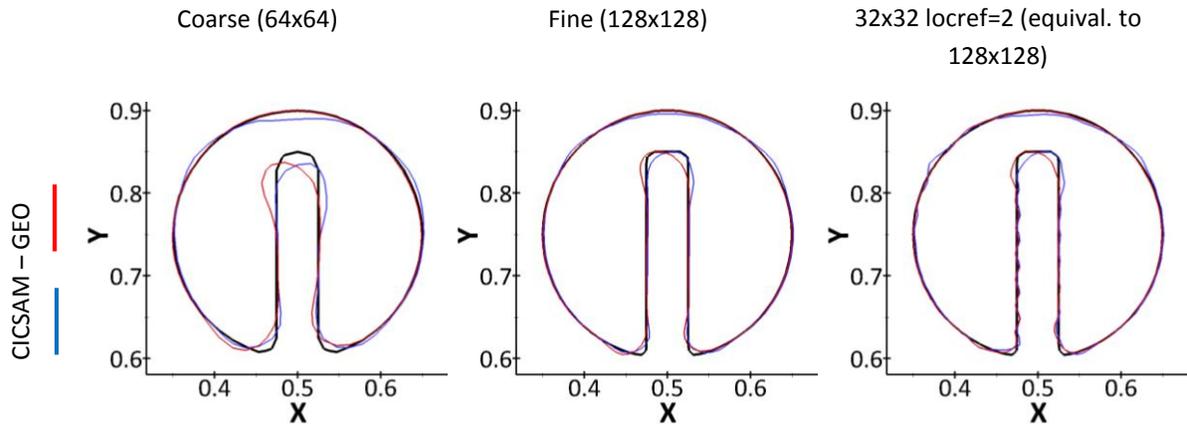

Figure 18. Use of Geo-Reconstruct in Benchmark case1, Zalesak's disk. Comparison between Geo-Reconstruct and CICSAM.

This Figure shows that Geo-Reconstruct and CICSAM provide similar results. Geo-Reconstruct may behave better at the liquid disk periphery, however it predicts higher deformation compared to CICSAM inside the disk's slot. Based on this benchmark case, it cannot be claimed that either one of these schemes behaves significantly better than the other.

Additionally, the performance of Geo-Reconstruct was tested in the case of droplet acceleration, in a case similar to cases 1a, 2a, 3a and 4a which are presented in Table 2. These cases are solved in the coarser grids encountered in this work (using four (4) levels of local refinement), while numbers 1-4 represent CICSAM,HRIC,HRIC+SHARP,HRIC+HSHARP methods referenced appropriately in the main body of this study. Results of the volume fraction contours, where values between 0.001 and 0.999 are plotted, are presented in Figure 19.

Based on the above results, it was observed that at some point during the simulation, particularly after 400ms of runtime, a small bubble started to form inside the droplet for unspecified reasons, proving that the use of Geo-Reconstruct may lead into unrealistic simulation results, at least for the conditions and grid resolution studied in this work. Therefore, CICSAM was selected to be the "non-diffusive" scheme for reasons of comparison against HRIC.
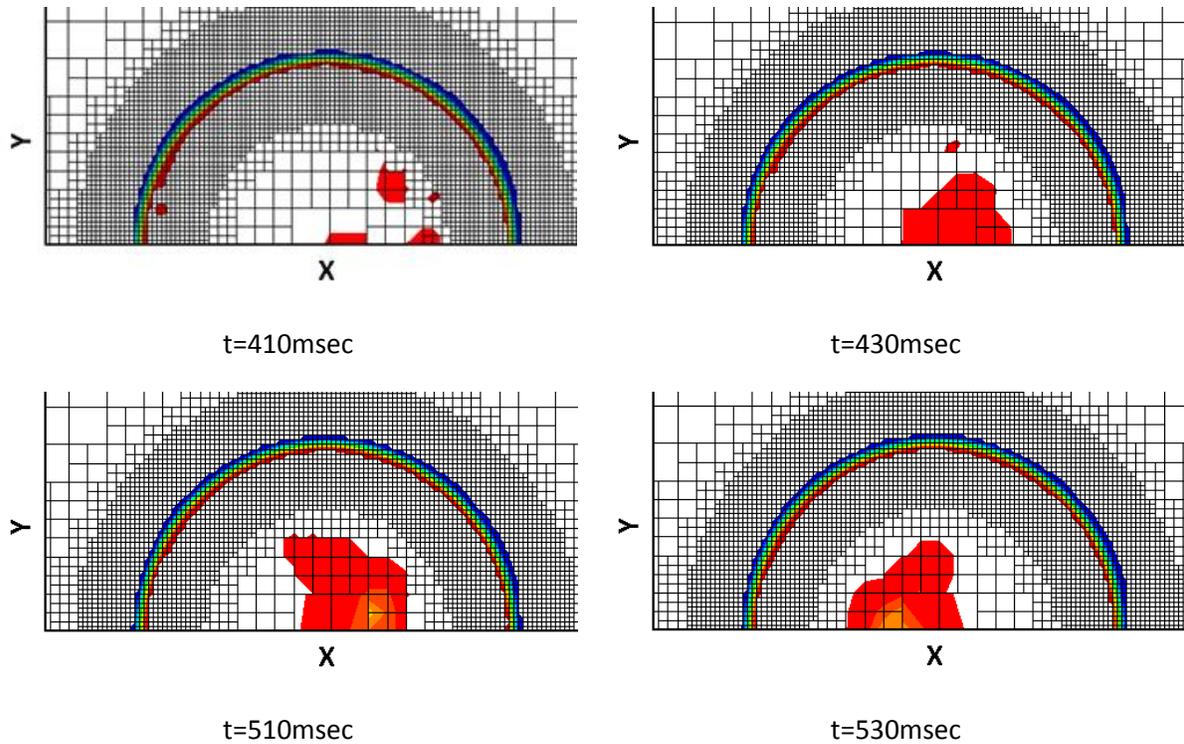
t=410msec

t=430msec

t=510msec

t=530msec

Figure 19. Time evolution of droplet acceleration using Geo-Reconstruct discretization scheme for volume fraction flux term. Contours of volume fraction are plotted, together with the respective computational grid. Volume fraction values between 0.001 and 0.999 are shown.

Appendix B. Validation of local refinement algorithm in a drop acceleration case

To justify the advantages of local grid refinement technique, the schemes of HRIC+HSHARP and CICSAM were both used on a one locally refined and its equivalent uniform grid. In the following Figures, the results obtained for both cases, are presented for the first 200ms of the phenomenon, where "loc" represents local refinement and "uni" represents the uniform grid.

CICSAM

HRIC

Figure 20. Temporal evolution of droplet velocity as calculated from CFD compared with the 1-D analytical solution. Cases CICSAM loc1,uni1, HRIC+HSHARP loc1,uni1.
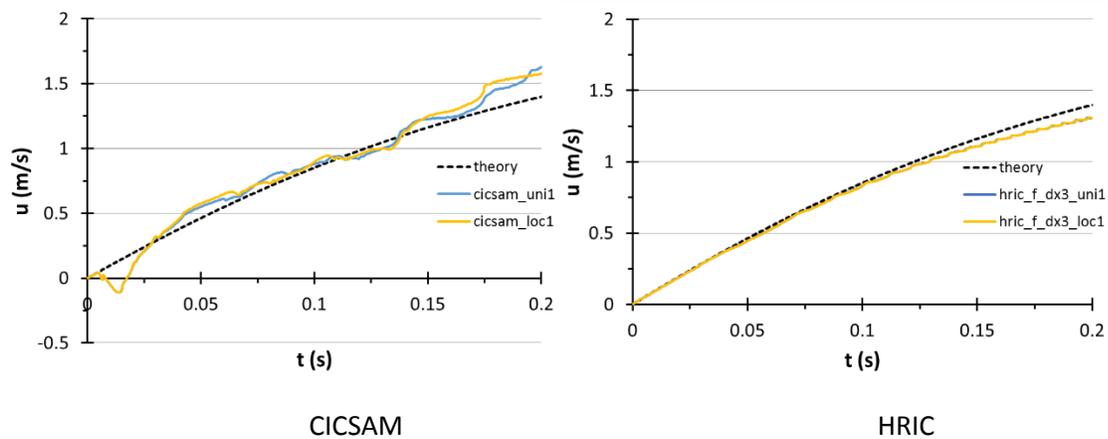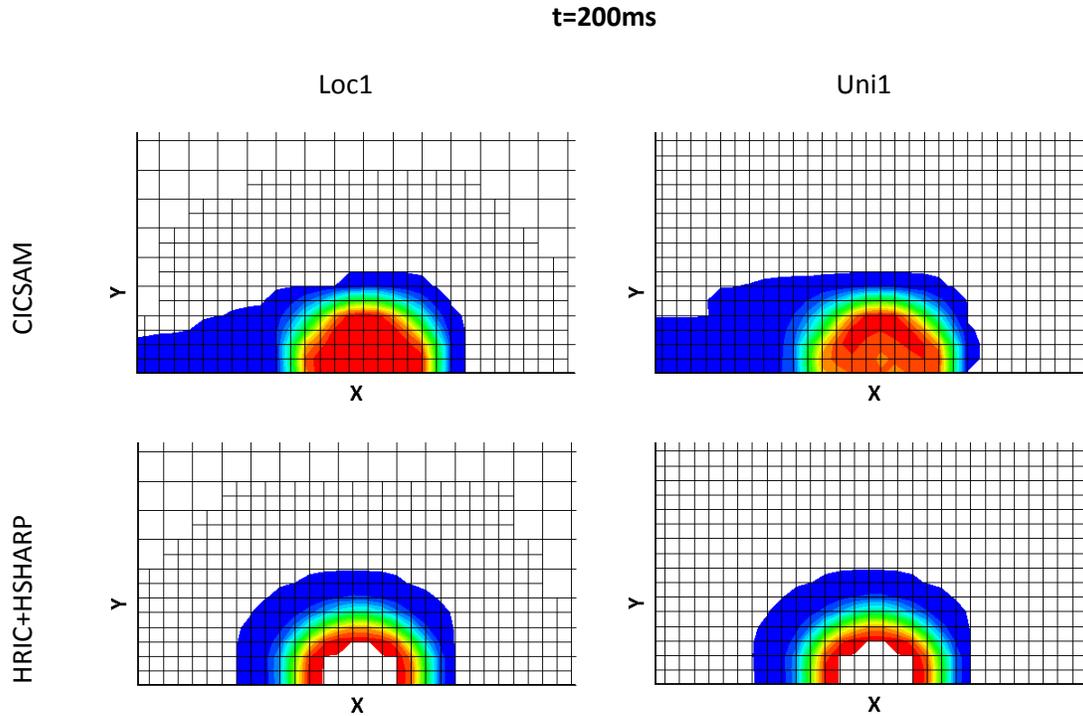
t=200ms

Figure 21. Temporal evolution of droplet velocity as calculated from CFD compared with the 1-D analytical solution. Cases CICSAM loc1,uni1, HRIC+HSHARP loc1,uni1.

The results indicate that the model is robust and that the predicted drop velocity using either the local refinement algorithm or the uniform refinement algorithm coincide, especially in the case of HRIC+HSHARP. In this case, additionally, the contour of volume fraction is almost identical. From these two observations, it is proved that the local refinement algorithm can provide with results almost identical when the color function is kept inside the high resolution area. Overall, the local refinement algorithm is proven to deliver similar results to the equivalent uniform grid cases, along with significant saving of computational resources. The cases of HRIC and HRIC+SHARP are not presented because the same conclusions apply.

References

1.   Miljkovic, N., et al., *Jumping-droplet-enhanced condensation on scalable superhydrophobic nanostructured surfaces.* Nano Letters, 2012. **13**(1): p. 179-187.
2.   Killion, J.D. and S. Garimella, *Simulation of Pendant Droplets and Falling Films in Horizontal Tube Absorbers.* Journal of Heat Transfer, 2005. **126**(6): p. 1003-1013.
3.   Han, Z., Z. Xu, and N. Trigui, *Spray/wall interaction models for multidimensional engine simulation.* International Journal of Engine Research, 2000. **1**(1): p. 127-146.
4.   Kim, J., *Spray cooling heat transfer: The state of the art.* International Journal of Heat and Fluid Flow, 2007. **28**(4): p. 753-767.
5.   Addy, H.E., *Ice accretions and icing effects for modern airfoils [microform] / Harold E. Addy, Jr*. NASA technical paper ; 210031., ed. N.G.R. Center2000, [Cleveland, Ohio] : [Springfield, Va: National Aeronautics and Space Administration, Glenn Research Center ; National Technical Information Service, distributor.

6.   Harlow, F.H. and J.E. Welch, *Numerical Calculation of Time‐Dependent Viscous Incompressible Flow of Fluid with Free Surface.* Physics of Fluids (1958-1988), 1965. **8**(12): p. 2182-2189.

7.   Harlow, F.H. and J.E. Welch, *Numerical Calculation of Time-Dependent Viscous Incompressible Flow of Fluid with Free Surface.* Physics of Fluids, 1965. **8**(12): p. 2182-2189.

8.   Fukai, J., et al., *Wetting effects on the spreading of a liquid droplet colliding with a flat surface: Experiment and modeling.* Physics of Fluids, 1995. **7**(2): p. 236-247.

9.   Zhao, Z., D. Poulikakos, and J. Fukai, *Heat transfer and fluid dynamics during the collision of a liquid droplet on a substrate—I. Modeling.* International Journal of Heat and Mass Transfer, 1996. **39**(13): p. 2771-2789.

10.   Manservisi, S. and R. Scardovelli, *A variational approach to the contact angle dynamics of spreading droplets.* Computers & Fluids, 2009. **38**(2): p. 406-424.

11.   Muradoglu, M. and S. Tasoglu, *A front-tracking method for computational modeling of impact and spreading of viscous droplets on solid walls.* Computers & Fluids, 2010. **39**(4): p. 615-625.

12.   Shin, S. and D. Juric, *Simulation of droplet impact on a solid surface using the level contour reconstruction method.* Journal of Mechanical Science and Technology, 2009. **23**(9): p. 2434-2443.

13.   Pasandideh-Fard, M., et al., *Capillary effects during droplet impact on a solid surface.* Physics of Fluids, 1996. **8**(3): p. 650-659.

14.   Pasandideh-Fard, M., et al., *Deposition of tin droplets on a steel plate: simulations and experiments.* International Journal of Heat and Mass Transfer, 1998. **41**(19): p. 2929-2945.

15.   Pasandideh-Fard, M., et al., *Cooling effectiveness of a water drop impinging on a hot surface.* International Journal of Heat and Fluid Flow, 2001. **22**(2): p. 201-210.

16.   Sikalo, S., et al., *Dynamic contact angle of spreading droplets: Experiments and simulations.* Physics of Fluids, 2005. **17**(6): p. 062103-13.

17.   Lunkad, S.F., V.V. Buwa, and K.D.P. Nigam, *Numerical simulations of drop impact and spreading on horizontal and inclined surfaces.* Chemical Engineering Science, 2007. **62**(24): p. 7214-7224.

18.   Strotos, G., et al., *Non-dimensionalisation parameters for predicting the cooling effectiveness of droplets impinging on moderate temperature solid surfaces.* International Journal of Thermal Sciences, 2011. **50**(5): p. 698-711.

19.   Nikolopoulos, N., A. Theodorakakos, and G. Bergeles, *A numerical investigation of the evaporation process of a liquid droplet impinging onto a hot substrate.* International Journal of Heat and Mass Transfer, 2007. **50**(1–2): p. 303-319.

20.   Yokoi, K., et al., *Numerical studies of the influence of the dynamic contact angle on a droplet impacting on a dry surface.* Physics of Fluids, 2009. **21**(7): p. 072102-12.

21.   Caviezel, D., C. Narayanan, and D. Lakehal, *Adherence and bouncing of liquid droplets impacting on dry surfaces.* Microfluidics and Nanofluidics, 2008. **5**(4): p. 469-478.

22.   Griebel, M. and M. Klitz, *Simulation of Droplet Impact with Dynamic Contact Angle Boundary Conditions.* INS Preprint No. 1302, 2013.

23.   Gunjal, P.R., V.V. Ranade, and R.V. Chaudhari, *Dynamics of drop impact on solid surface: Experiments and VOF simulations.* AIChE Journal, 2005. **51**(1): p. 59-78.

24.   Bussmann, M., S. Chandra, and J. Mostaghimi, *Modeling the splash of a droplet impacting a solid surface.* Physics of Fluids, 2000. **12**(12): p. 3121-3132.

25.   Roisman, I.V., et al., *Drop impact onto a dry surface: Role of the dynamic contact angle.* Colloids and Surfaces A: Physicochemical and Engineering Aspects, 2008. **322**(1–3): p. 183-191.

26.   Francois, M. and W. Shyy, *Computations of drop dynamics with the immersed boundary method, Part 2: Drop impact and heat transfer.* Numerical Heat Transfer, Part B: Fundamentals, 2003. **44**(2): p. 119-143.

27.   Ganesan, S., *On the dynamic contact angle in simulation of impinging droplets with sharp interface methods.* Microfluidics and Nanofluidics, 2013. **14**(3-4): p. 615-625.

28. Singh, R., *Three-dimensional marker-based multiphase flow computation using adaptive Cartesian grid techniques*, 2006, University of Florida.

29. Ubbink, O., *Numerical prediction of two fluid systems with sharp interfaces*, 1997, Imperial College.

30. Muzaferija, S., et al., *A Two-Fluid Navier-Stokes Solver to Simulate Water Entry.* 22nd Symposium on Naval Hydrodynamics, Washington, DC,, 1998: p. 638-651.

31. Wacławczyk, T. and T. Koronowicz, *Comparison of CICSAM and HRIC High-Resolution Schemes for interface capturing.* Journal of Theoretical and Applied Mechanics, 2008. **46**(2): p. 325-345.

32. Olsson, E. and G. Kreiss, *A conservative level set method for two phase flow.* Journal of Computational Physics, 2005. **210**(1): p. 225-246.

33. Olsson, E., G. Kreiss, and S. Zahedi, *A conservative level set method for two phase flow II.* Journal of Computational Physics, 2007. **225**(1): p. 785-807.

34. Sato, Y. and B. Ničeno, *A conservative local interface sharpening scheme for the constrained interpolation profile method.* International Journal for Numerical Methods in Fluids, 2012. **70**(4): p. 441-467.

35. Shukla, R.K., C. Pantano, and J.B. Freund, *An interface capturing method for the simulation of multi-phase compressible flows.* Journal of Computational Physics, 2010. **229**(19): p. 7411-7439.

36. Weller, H.G., *A new approach to VOF-based interface capturing methods for incompressible and compressible flow*2008, Technical Report TR/HGW/04: Open CFD Ltd.

37. Berberovic, E., *Investigation of Free-surface Flow Associated with Drop Impact: Numerical Simulations and Theoretical Modeling*, 2010, TU Darmstadt / FG Strömungslehre und Aerodynamik.

38. So, K.K., X.Y. Hu, and N.A. Adams, *Anti-diffusion method for interface steepening in two-phase incompressible flow.* Journal of Computational Physics, 2011. **230**(13): p. 5155-5177.

39. So, K.K., X.Y. Hu, and N.A. Adams, *Anti-diffusion interface sharpening technique for two-phase compressible flow simulations.* Journal of Computational Physics, 2012. **231**(11): p. 4304-4323.

40. Lentine, M., et al., *Simulating free surface flow with very large time steps*, in *Proceedings of the 11th ACM SIGGRAPH / Eurographics conference on Computer Animation*2012, Eurographics Association: Lausanne, Switzerland. p. 107-116.

41. Hirt, C.W. and B.D. Nichols, *Volume of fluid (VOF) method for the dynamics of free boundaries.* Journal of Computational Physics, 1981. **39**(1): p. 201-225.

42. Nikolopoulos, N., A. Theodorakakos, and G. Bergeles, *Normal impingement of a droplet onto a wall film: a numerical investigation.* International Journal of Heat and Fluid Flow, 2005. **26**(1): p. 119-132.

43. Strotos, G., et al., *Numerical investigation on the evaporation of droplets depositing on heated surfaces at low Weber numbers.* International Journal of Heat and Mass Transfer, 2008. **51**(7–8): p. 1516-1529.

44. Brackbill, J.U., D.B. Kothe, and C. Zemach, *A continuum method for modeling surface tension.* Journal of Computational Physics, 1992. **100**(2): p. 335-354.

45. Nikolopoulos, N., K.S. Nikas, and G. Bergeles, *A numerical investigation of central binary collision of droplets.* Computers & Fluids, 2009. **38**(6): p. 1191-1202.

46. Nikolopoulos, N., A. Theodorakakos, and G. Bergeles, *Three-dimensional numerical investigation of a droplet impinging normally onto a wall film.* Journal of Computational Physics, 2007. **225**(1): p. 322-341.

47. Strotos, G., et al., *Numerical investigation of the cooling effectiveness of a droplet impinging on a heated surface.* International Journal of Heat and Mass Transfer, 2008. **51**(19–20): p. 4728-4742.

48. Strotos, G., et al., *Cooling effectiveness of droplets at low Weber numbers: Effect of temperature.* International Journal of Thermal Sciences, 2013. **72**(0): p. 60-72.

49.   Zahedi, S., K. Gustavsson, and G. Kreiss, *A conservative level set method for contact line dynamics.* Journal of Computational Physics, 2009. **228**(17): p. 6361-6375.

50.   Sato, Y. and B. Ničeno, *A new contact line treatment for a conservative level set method.* Journal of Computational Physics, 2012. **231**(10): p. 3887-3895.

51.   Theodorakakos, A. and G. Bergeles, *Simulation of sharp gas–liquid interface using VOF method and adaptive grid local refinement around the interface.* International Journal for Numerical Methods in Fluids, 2004. **45**(4): p. 421-439.

52.   Zalesak, S., *Fully multidimensional flux-corrected transport algorithms for fluids.* J. Comput. Phys., 1979. **31**: p. 335-362.

53.   Rider, W.J. and D.B. Kothe, *Reconstructing Volume Tracking.* Journal of Computational Physics, 1998. **141**(2): p. 112-152.

54.   Clift, R., J.R. Grace, and M.E. Weber, *Bubbles, drops, and particles*, ed. J.R. Grace and M.E. Weber1978, New York: Academic Press.

55.   Feng, Z.-G. and E.E. Michaelides, *Drag Coefficients of Viscous Spheres at Intermediate and High Reynolds Numbers.* Journal of Fluids Engineering, 2001. **123**(4): p. 841-849.

56.   Ryu, S.-Y. and S.-H. Ko, *A COMPARATIVE STUDY OF LATTICE BOLTZMANN AND VOLUME OF FLUID METHOD FOR TWO-DIMENSIONAL MULTIPHASE FLOWS.* Nuclear Engineering and Technology, 2012. **44**(6): p. 623-638.